Controls of shear zone rheology and tectonic loading on postseismic creep

Laurent G. J. Montési
Woods Hole Oceanographic Institution, Woods Hole, Massachusetts, USA

Received 2 December 2003; revised 25 June 2004; accepted 22 July 2004; published 8 October 2004.

[1] Postseismic deformation is well documented in geodetic data collected in the aftermath of large earthquakes. In the postseismic time interval, GPS is most sensitive to creep in the lower crust or upper mantle activated by earthquake-generated stress perturbations. In these regions, deformation may be localized on an aseismic frictional surface or on a ductile shear zone. These two hypotheses imply specific rheologies and therefore time dependence of postseismic creep. Hence postseismic creep constitutes a potential probe into the rheology of aseismic regions of the lithosphere. I present a simple shear zone model of postseismic creep in which the rheology of the creeping element can be varied. In the absence of tectonic loading during the postseismic time interval, the displacement history of the shear zone obeying a power law rheology with stress exponent n follows an analytical relaxation curve parameterized by $1/n$. For a frictional surface, postseismic creep follows the same relaxation law in the limit $1/n \rightarrow 0$. A rough estimate of the apparent stress exponent can be obtained from continuous GPS records. Application to data collected after the 1994 Sanriku earthquake yields $1/n \sim 0.1$, which is consistent with dislocation creep mechanisms. However, the records of two other subduction zone events, the 2001 Peru event and the 1997 Kronotski earthquake, and a continental strike-slip earthquake, the 1999 İzmit earthquake, require negative $1/n$. Rather than characterizing the shear zone rheology, these negative exponents indicate that reloading of the shear zone by tectonic forces is important. Numerical simulations of postseismic deformation with nonnegligible reloading produce curves that are well fit by the generalized relaxation law with $1/n < 0$, although the actual stress exponent of the rheology is positive. While this prevents rheology from being tightly constrained by the studied GPS records, it indicates that reloading is important in the postseismic time interval. In other words, the stress perturbation induced by an earthquake is comparable to the stress supported by ductile shear zones in the interseismic period. *INDEX TERMS:* 1242 Geodesy and Gravity: Seismic deformations (7205); 1236 Geodesy and Gravity: Rheology of the lithosphere and mantle (8160); 8159 Tectonophysics: Rheology—crust and lithosphere; 8164 Tectonophysics: Stresses—crust and lithosphere; 3220 Mathematical Geophysics: Nonlinear dynamics; *KEYWORDS:* postseismic, rheology, stress

Citation: Montési, L. G. J. (2004), Controls of shear zone rheology and tectonic loading on postseismic creep, *J. Geophys. Res.*, *109*, B10404, doi:10.1029/2003JB002925.

1. Introduction

[2] The earthquake cycle is commonly divided into three time intervals: a loading period, the earthquake rupture itself (coseismic period) and the postseismic period. Deformation of the lithosphere in the postseismic interval is evidenced not only by aftershocks but also by aseismic deformation that liberates an energy sometimes comparable to the earthquake itself, overpowering the energy released by aftershocks [e.g., *Savage and Svarc*, 1997; *Heki et al.*, 1997; *Yagi et al.*, 2001; *Ergintav et al.*, 2002]. Aseismic postseismic deformation, or postseismic creep, is now recognized as a major component of the earthquake cycle, influencing triggering of earthquakes at regional and global scale [*Pollitz et al.*, 1998a; *Freed and Lin*, 2001; *Chéry et al.*, 2001; *Casarotti et al.*, 2001] and affecting paleoseismicity and earthquake risk estimates [*Freed and Lin*, 2002]. Various mechanical origins for postseismic creep have been proposed, ranging from poroelastic rebound [*Peltzer et al.*, 1998; *Pollitz et al.*, 2001; *Jónsson et al.*, 2003], continued slip on the earthquake rupture area (i.e., afterslip [*Marone et al.*, 1991]), to distributed or localized deformation in a ductile lower crust or upper mantle [*Deng et al.*, 1998; *Savage et al.*, 1994; *Reilinger et al.*, 2000; *Bürgmann et al.*, 2002; *Freed and Bürgmann*, 2004]. This study explores how tectonic loading and the rheology of the region that produces postseismic creep influence the time dependence of postseismic creep.

0148-0227/04/2003JB002925$09.00

[3] Because of its aseismic character, postseismic creep can be observed only through geodetic means. Space geodesy, in particular, Global Positioning System (GPS) and interferometric synthetic aperture radar (InSAR), has become the tool of choice to study postseismic creep. Postseismic creep has now been detected after many large earthquakes occurring in well-instrumented areas, although not by any means all of them. For instance, *Melbourne et al.* [2002] show that even in GPS time series with fine temporal resolution, no postseismic signal could be detected following the 1995 Antofagasta, Chile, earthquake.

[4] Geodetic data can be used to constrain where postseismic deformation occurs. When inverting postseismic displacement, it is commonly assumed that deformation occurs on a shear zone or fault plane of specified geometry, often similar to the seismogenic fault but possibly larger in extent [*Oppenheimer et al.*, 1990; *Shen et al.*, 1994; *Bürgmann et al.*, 1997; *Donnellan and Lyzenga*, 1998; *Bürgmann et al.*, 2001]. Inversion of a network of geodetic stations can constrain spatial variations in the amount of postseismic deformation on the shear zone [*Pollitz et al.*, 1998b; *Reilinger et al.*, 2000; *Bechor et al.*, 2001; *Yagi et al.*, 2001; *Bürgmann et al.*, 2002; *Hsu et al.*, 2002; *Owen et al.*, 2002; *Zweck et al.*, 2002; *Miyazaki et al.*, 2003; *Yu et al.*, 2003]. Repeated surveys and most importantly continuous GPS stations resolve not only the spatial variation but also the time dependence of postseismic creep [*Bürgmann et al.*, 2002]. Postseismic creep often occurs in the down-dip continuation of the fault plane, and decays over time. This implies a model of the lithosphere with shallow seismogenic behavior and deeper aseismic behavior activated by earthquake-generated stress perturbations.

[5] The transition from seismogenic to aseismic behavior with depth may correspond to the brittle-ductile transition long documented in rock mechanics experiments [e.g., *Brace and Kohlstedt*,1980]. In the laboratory, ductile creep remains distributed, leading to the expectation of distributed deformation below the seismogenic zone. However, geological studies have shown repeatedly that ductile deformation is in fact localized on ductile shear zones [e.g., *Ramsay*, 1980; *Vauchez and Tommasi*, 2003]. Localization in the ductile field corresponds to a reduced grain size or a different mineral assemblages (including hydrated minerals) in the shear zones [*White and Knipe*, 1978; *Sibson*, 1986; *Fitz Gerald and Stünitz*, 1993; *Jin et al.*, 1998]. Individual strands of localized ductile shear zones are activated only for a short amount of time before being abandoned [*Sibson*, 1980; *Hobbs et al.*, 1986]. The high stress recorded in shear zones suggests a link between shear zone dynamics and earthquakes [*Küster and Stöckhert*, 1999; *Trepmann and Stöckhert*, 2003]. Although forming a localized ductile shear zone without external forcing is notoriously difficult [*Poirier*, 1980; *Montési and Zuber*, 2002; *Regenauer-Lieb and Yuen*, 2003], repeated earthquakes can result in a long-term grain size reduction in their down-dip termination, which helps localization [*Montési and Hirth*, 2003]. Therefore it is reasonable to assume the presence of a localized ductile shear zone in the down-dip continuation of the seismogenic zone.

[6] An alternative hypothesis is that the behavior of the rocks below the seismogenic zone is still brittle, with deformation occurring along a frictional surface but that the increased temperature at depth changes the constitutive behavior of the friction from velocity weakening to velocity strengthening [*Brace and Byerlee*, 1970; *Tse and Rice*, 1986]. As velocity-strengthening friction is inherently stable, it does not produce earthquakes. Instead, an earthquake-induced increase in the applied stress simply increases the slip rate. Differentiating between a velocity-strengthening frictional surface and a ductile shear zone model of postseismic creep requires models that are sensitive to details of the assumed material rheology.

[7] *Hearn et al.* [2002] model postseismic deformation following the 1999 İzmit earthquake using several rheological models of the extended fault plane to determine what type of rock behavior is most likely responsible for postseismic creep. They conclude that the data are most compatible with velocity-strengthening friction. However, the variance reduction of that model is only slightly better than can be achieved with a linear viscous model. All these models predict a deep patch with high deformation rate that does not appear in the kinematic inversions of *Bürgmann et al.* [2002]. From that study, it may be concluded that patterns of postseismic deformation have little sensitivity to the rheology of the shear zone. It is shown below that the time decay of postseismic deformation can help constrain shear zone rheology.

[8] In section 2, I present a simple spring-slider model used to predict the time dependence of postseismic creep. The rheology of the slider element in this model can be adjusted to represent viscous and frictional processes, among others. The postseismic deformation history in these models is parameterized by an apparent stress exponent characteristic of the shear zone rheology. However, tectonic loading during the postseismic time period modifies the displacement history of the shear, affecting the rheological inferences made from GPS data. This model is fitted to GPS data first from subduction zone earthquakes [*Heki et al.*, 1997; *Bürgmann et al.*, 2001; *Melbourne et al.*, 2002], then from the 1999 İzmit earthquake [*Ergintav et al.*, 2002; *Bürgmann et al.*, 2002]. The inferred values of the stress exponent indicate that the behavior of the lithosphere in the postseismic interval is probably non-Newtonian and that tectonic loading cannot be ignored.

2. A Spring-Slider Relaxation Model for Postseismic Deformation

[9] The motion of a fault during an earthquake perturbs the state of stress of the surrounding crust through elastic interactions. After a transition period during which elastic waves propagate, the stress perturbation reaches a static value. If the lithosphere deforms plastically or viscously, the stress change induces a flow field. As the crust deforms, it relaxes the stress generated by the earthquake. Therefore this postseismic response to earthquake-generated stress perturbation is best described as a relaxation. The details of this relaxation depend on the rheology of the deforming rocks.

[10] We consider three candidate rheologies to describe the behavior of rocks in the postseismic time interval, velocity-strengthening friction, Newtonian viscosity, and ductile creep. These rheologies are presented below and then included in a simple model of postseismic deformation.

This section shows how the different rheologies affect postseismic creep.

2.1. Shear Zone Rheologies

2.1.1. Velocity-Strengthening Friction

[11] Laboratory experiments show that the shear stress σ supported by a frictional surface is a function of the displacement rate of that surface, V_S, and at least one state variable [*Dieterich*, 1978; *Ruina*, 1983; *Scholz*, 2002]. If the evolution of the state variable is assumed to be rapid, a steady state friction law can be written as

$$V_S = V_c \exp\left(\frac{\sigma - \sigma_c}{C}\right), \tag{1}$$

with V_c, σ_c, and C, three material constants; σ_c is the stress supported by the fault if sliding at velocity V_c.

[12] If $C < 0$, the surface obeys velocity-weakening friction, which is unstable, a necessary condition for seismogenic behavior [*Rice and Ruina*, 1983; *Dieterich*, 1992]. If $C > 0$, the surface obeys velocity-strengthening friction, which is stable, but can generate postseismic creep. Laboratory experiments indicate a transition from velocity-weakening to velocity-strengthening friction with increasing temperature, which might control the down-dip limit of seismicity in continental areas [*Brace and Byerlee*, 1970; *Stesky et al.*, 1974; *Tse and Rice*, 1986; *Blanpied et al.*, 1991, 1998; *Scholz*, 2002].

2.1.2. Ductile Creep

[13] Alternatively, the rheological transition that limits seismogenic behavior at depth may be one from brittle to ductile behavior [e.g., *Brace and Kohlstedt*, 1980]. A ductile rheology commonly observed in the laboratory is power law creep, whereby the strain rate of a rock sample, $\dot{\varepsilon}$, is proportional to the applied stress to a power n. Motion of intracrystalline dislocations leads to power law creep with $3 < n < 5$.

[14] Although ductile creep is distributed over a whole sample in laboratory experiments, it is localized in shear zones in nature [e.g., *Ramsay*, 1980; *Vauchez and Tommasi*, 2003]. If we assume that ductile creep in the postseismic time interval occurs in a shear zone of thickness H, the velocity across this shear zone is

$$V_S = AH\sigma^n, \tag{2}$$

where A is a preexponential factor that depends in general on temperature and chemical environment [*Evans and Kohlstedt*, 1995]. Grain boundary sliding accommodated by dislocation creep is also described by equation (2) with A depending on grain size and $n \sim 3$ [*Hirth and Kohlstedt*, 2003]. Here again, the stress σ is the shear stress on the shear zone. In laboratory studies, equation (2) is often written for a differential stress and the temperature dependence of the flow law is separated from the parameter A. Hence the value of A in equation (2) is different from that reported in laboratory studies. Simple geometrical considerations allow the conversion of laboratory values to those in equation (2). Regardless, the exact value of A has no importance for this work as I concentrate on evaluating the functional form of the rheology under natural conditions.

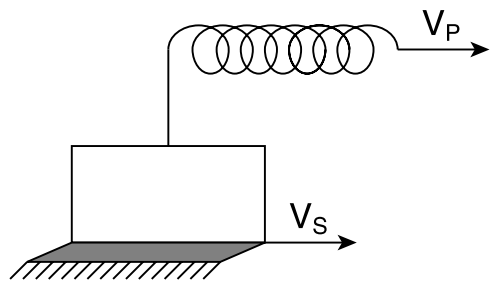

Figure 1. Conceptual model of postseismic deformation. A creeping shear zone (shaded) is loaded elastically with a load point velocity V_P. During interseismic intervals, V_P is dominated by a remote tectonic loading. However, earthquakes load adjacent regions of the lithosphere, including a nearby shear zone, which responds to this loading by enhanced postseismic creep.

2.1.3. Viscous Flow

[15] A particular case of equation (2) arises for $n = 1$. This defines Newtonian, or linear, viscous flow

$$V_S = AH\sigma. \tag{3}$$

In this case, A is simply the viscosity of the material. Equation (3) is appropriate for rocks deforming by grain boundary sliding accommodated by diffusion creep [*Evans and Kohlstedt*, 1995], in which case A depends on grain size as well as temperature and chemical environment.

[16] Viscous flow is commonly assumed in fluid mechanics, as it is appropriate for water. Most simple geodynamics models are also built on the assumption of viscous flow, even though rock behavior is usually more complex.

2.2. Generalized Relaxation Law

[17] Deformation of a frictional or ductile shear zone reduces the stress originally applied on it, while tectonic loading or earthquakes increase the applied stress. Let us simplify the interaction between seismogenic and aseismic shear zones as shown in Figure 1. The shear zone deforms at velocity V_S. It is loaded by a combination of tectonic and earthquake-induced stresses increasing at the rate $\dot{\sigma}_P$, alternatively represented by a load point velocity V_P transmitted to the shear zone through a spring of stiffness K. The stressing rate and load point velocity are related by $\dot{\sigma}_P = KV_P$. Geometrical complexity between stress sources and the shear zone are absorbed in the value of K. In general, both V_S and V_P are time-dependent.

[18] In this parameterized model, the change in shear stress applied on the fault is given by

$$d\sigma/dt = K(V_P - V_S). \tag{4}$$

The shear zone velocity V_S can be replaced in the coupling equation (4) by the appropriate constitutive relation chosen between equations (1) and (3). Then, equation (4) is transformed into a differential equation for σ, or substituting again the rheology, a differential equation for shear zone velocity V_S. The solution of this equation with initial condition $V_S = V_0$ at $t = 0$ provides an expression for the displacement history of the shear zone.

Table 1. Summary of Rheological Laws and Postseismic and Velocity History

	Definition	Velocity-Strengthening Friction	Ductile Creep	Viscous Flow
Rheology	$V_S(\sigma)$	$V_c \exp(\frac{\sigma-\sigma_c}{C})$	$AH\sigma^n$	$AH\sigma$
Velocity history	$V_S(t)/V_0$	$[1 + t/\tau]^{-1}$	$[1 + (1 - 1/n)t/\tau]^{-\frac{1}{(1-1/n)}}$	$\exp(-t/\tau)$
Displacement history	$\frac{D_S(t)-D_0}{V_0\tau}$	$\log(1 + t/\tau)$	$n\{1 - [1 + (1 - 1/n)t/\tau]^{\frac{1}{1-n}}\}$	$[1 - \exp(-t/\tau)]$
τ	$\left.\frac{V_S}{dV_S/dt}\right\|_{t=0}$	$\frac{C}{KV_0}$	$\frac{1}{n}V_0{}^{-1+1/n}K^{-1}(AH)^{-1/n}$	$(KAH)^{-1}$

[19] The relation between the velocity history obtained for different rheologies is made clear by consideration of the nondimensional version of the velocity evolution equation. Velocities are scaled by the shear zone velocity V_0 at time $t = 0$ (immediately after the earthquake), and time is scaled by a suitably chosen factor τ defined below.

[20] We obtain for a frictional rheology (equation (1))

$$dV_S^*/dt^* = V_S^*\left(V_P^* - V_S^*\right), \tag{5}$$

$$1/\tau = KV_0/C, \tag{6}$$

where the asterisks indicate nondimensional quantities and τ was chosen to cancel all the constants in the velocity evolution equation. However, τ also has a physical meaning, being the ratio of shear zone velocity and acceleration at time $t = 0$ for the case $V_P = 0$.

[21] For a power law rheology (equation (2)), we obtain

$$dV_S^*/dt^* = V_S^{*1-1/n}\left(V_P^* - V_S^*\right), \tag{7}$$

$$1/\tau = nK(AH)^{1/n}V_0^{1-1/n}. \tag{8}$$

Comparing equations (4) and (7) reveals that the frictional case is functionally identical to the power law case in the limit $1/n \rightarrow 0$.

[22] The Newtonian case corresponds to the limit $1/n \rightarrow 1$. In that case, we obtain

$$dV_S^*/dt^* = V_P^* - V_S^*, \tag{9}$$

$$1/\tau = KAH. \tag{10}$$

The Newtonian rheology is the only one considered here for which τ depends only on constitutive parameters, not the initial velocity V_0.

[23] During an earthquake, the loading velocity is comparable to the sliding velocity, but in the postseismic interval, it represents tectonic loading, which is much slower. If the rate of tectonic loading is negligible in the postseismic interval with respect to the shear zone velocity, the velocity evolution equation (equation (7), (5), or (9)) can be solved analytically, subject to the initial condition $V_S^* = 1$ at $t = 0$. This solution can be integrated over time to give the nondimensional shear zone displacement history $D_S^*(t^*)$. The dimensional displacement is given by $D_S(t) = D_0 + V_0\tau D_S^*(t/\tau)$. V_0 is defined as the shear zone velocity at the beginning of the time interval considered, i.e., immediately after the earthquake. The last integration constant, D_0, is an arbitrary initial displacement of the shear zone at $t = 0$. The solutions for the rheologies described above are compiled in Table 1.

[24] As the frictional and viscous cases are simply end-members of the power law case, the general relaxation law obtained for ductile creep constitutes a master curve, parameterized by D_0, V_0, τ, and $1/n$, which describes a range of behavior ranging from viscous flow ($1/n \rightarrow 1$) to frictional sliding ($1/n \rightarrow 0$).

[25] This general relaxation law is

$$V_S = V_0[1 + (1 - 1/n)t/\tau]^{-1/(1-1/n)}, \tag{11a}$$

$$D_S = D_0 + nV_0\tau\left\{1 - [1 + (1 - 1/n)t/\tau]^{1/(1-n)}\right\}. \tag{11b}$$

Note that the velocity and displacement curves are defined for negative values of $1/n$, but not if $1/n > 1$ and the time exceeds a critical value. The general relaxation law is graphed in Figure 2 for various values of $1/n$. The effect of the stress exponent is to change the curvature of these functions. Postseismic creep ceases earlier for viscous behavior.

[26] The inverse stress exponent $1/n$ characterizes the rheology involved in postseismic creep. It is tempting to draw a parallel between this stress exponent and the concept of effective stress exponent, n_e, described by *Smith* [1977] and *Montési and Zuber* [2002]. However, such a parallel would be misleading. In the study by *Montési and Zuber* [2002], the effective stress exponent is a measure of the nonlinearity of a rheological system. It is defined for a particular applied stress and loses its validity as the loading conditions change. For instance, the effective stress exponent for velocity-strengthening friction is $1/n_e = C/\sigma$ (with the notation of this paper), which is a function of time in the postseismic interval. By contrast, the inverse stress exponent required in equation (11) to recover frictional behavior is $1/n = 0$. It does not depend on time. The stress exponent in equation (11) characterizes the entire postseismic relaxation curve, not the rheology at any particular condition. Therefore $1/n < 0$ does not imply localization, as $1/n_e < 0$ does [*Montési and Zuber*, 2002]. Negative values of $1/n$ are allowed in equation (11). In fact, these values will be required by some of the records of postseismic deformation examined below. It is shown below that $1/n < 0$ probably indicate significant reloading of the shear zone in the postseismic period.

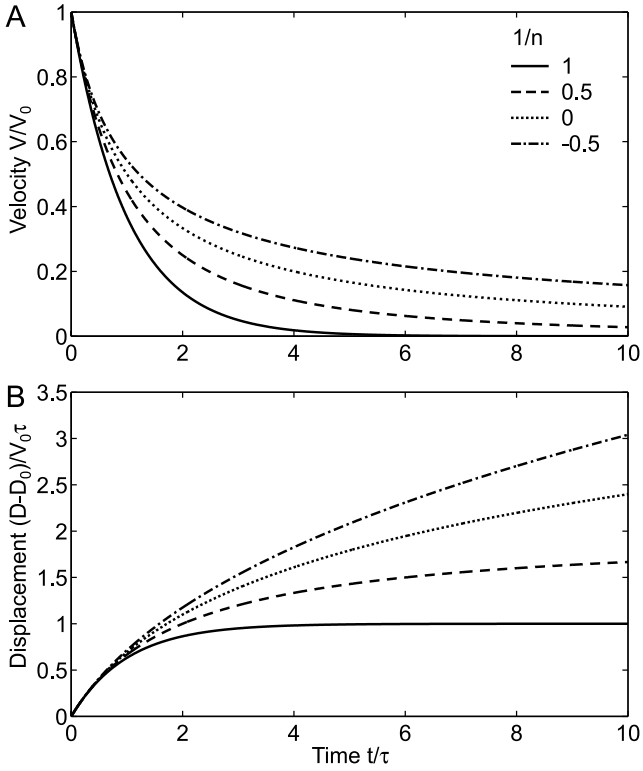

Figure 2. History of (a) velocity and (b) displacement of a shear zone following an earthquake-induced stress perturbation according to the general relaxation law (equation (11)), ignoring reloading velocity. Solid line is Newtonian viscous rheology ($1/n \rightarrow 1$); dashed line is non-Newtonian creep ($1/n = 0.5$); dotted line is frictional sliding ($1/n = 0$); dash-dotted line is $1/n = -0.5$. Other input parameters are $D_0 = 0$, $V_0 = 1$, and $\tau = 1$, so that all curves have the same initial behavior. The stress exponent influences the rate at which postseismic motion decays.

[27] At first sight, it may look incongruous that the velocity history for the frictional rheology is obtained from the power law case when $1/n \rightarrow 0$, as equation (2) implies that σ independent of V_S in that limit, evidently a different relation than equation (1). To understand the origin of this apparent discrepancy, one needs to consider the effect of taking the limit $1/n \rightarrow 0$ on the time constant τ and its relation with the rheological parameters such as C. As $1/n \rightarrow 0$, τ, defined for a power law rheology by equation (8), goes to 0. Using now the relation between τ and the rheological parameters for frictional sliding (equation (6)), this implies $C \rightarrow 0$. In that limit, in equation (1), the stress is independent on shear zone velocity. This is consistent with taking the limit of equation (2) with $1/n \rightarrow 0$. For other values of C, the limit $1/n \rightarrow 0$ must be taken with τ fixed. For that doing, it is necessary to abandon the relation of τ with the constitutive parameters (equations (8) and (6)). This poses no difficulty for the time evolution of postseismic creep as τ is rigorously defined as the ratio of acceleration to velocity at $t = 0$, a kinematic definition.

[28] The stress history can also be derived in a consistent manner for both power law and frictional rheologies using the coupling equation (equation (4)) rather than the rheology. Integrating equation (4) relates stress changes to the difference between shear zone displacement D_S and loading $V_P t$:

$$\sigma^*(t^*) - \sigma^*(0) = \int_0^{t^*} V_P^* dt^* + d^*(0) - d^*(t^*). \tag{12}$$

The stress scale is $\sigma_0 = K\tau V_0$. For the simple case where $V_P = 0$, Table 1 reveals that indeed, displacement is proportional to the $\log(V_S)$ for the case $1/n \rightarrow 0$ and to $V_S^{1/n}$ otherwise.

[29] The relaxation laws assume a simple coupling system with an external loading (Figure 1) and a rheology for the shear zone. This approach is similar to that of *Dieterich* [1994] to calculate the slip rate history during the nucleation phase of an earthquake. However, Dieterich used a different constitutive relation. Where I have used friction laws in steady state, he considers explicitly the time evolution of the state variable. To derive his equations (A9) to (A12), he makes the assumption that the displacement rate on the seismogenic fault is much larger than D_{Ci}/θ_i, where θ_i is one of a set of state variables and D_{Ci} the characteristic distance over which this variable evolves. Under this assumption, the state variable changes exponentially with slip distance, which implies a linear dependence of the shear stress supported by the fault on displacement. With the simple coupling system described in equations (4) and (12), also used by *Dieterich* [1994], stress varies linearly with displacement. The effects of the state variable and external coupling can therefore be combined. The result is an evolution equation similar to that used in this work (equations (5) and (6)), albeit with a modified stiffness K and parameter C. This implies an interesting symmetry between precursory slip and postseismic creep if the latter is due to velocity-strengthening sliding. They should obey a similar functional form but with different timescales τ.

[30] The time constant τ has different interpretations depending on the assumed rheology (Table 1). However, it is consistently defined as the ratio of shear zone velocity and acceleration at time 0. As such, it depends on the initial velocity, except for the viscous flow law (Table 1). A change in the time origin therefore changes the apparent values of τ

$$D_S(t, \{D_0, V_0, \tau, 1/n\}) = D_S(t_1, \{D_1, V_1, \tau_1, 1/n\}), \tag{13}$$

with

$$t_1 = t - t_0, \tag{14a}$$

$$D_1 = D_0 + nV_0\tau\left\{1 - [1 + (1 - 1/n)t_0/\tau]^{1/(1-n)}\right\}, \tag{14b}$$

$$V_1 = V_0(t_0/\tau)^{n/(1-n)}, \tag{14c}$$

$$\tau_1 = \tau - (1 - 1/n)t_0. \tag{14d}$$

[31] Many studies have revealed different time constants for postseismic creep at short and long timescale,

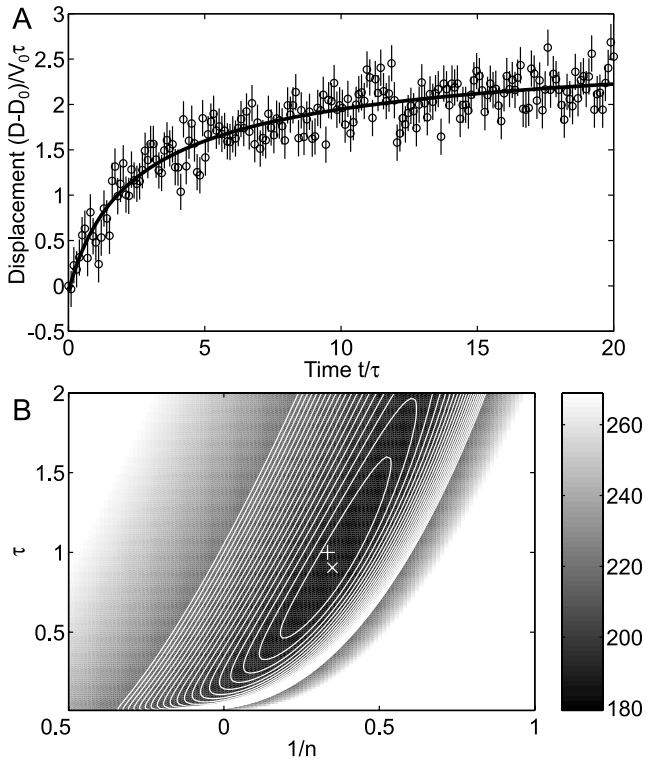

Figure 3. Inversion results for a simulated postseismic history with $1/n = 1/3$, $D_0 = 0$, $V_0 = 1$, $\tau = 1$, and random noise following a normal distribution with standard deviation of 0.2. (a) Simulated data set (circles with error bars) and the best fit obtained by the Levenberg-Marquart method (solid line), which gives $1/n = 0.352$, $D_0 = 0.01$, $V_0 = 1.14$, and $\tau = 0.919$. (b) Least misfit obtained for test values of $1/n$ and τ. There is a strong correlation between the uncertainty on these two parameters. Best fit is marked by the cross, and the original value is marked by the plus.

which are interpreted sometimes as different rheologies or deformation mechanisms. However, it is clear that if the rheology is nonlinear, different τ are expected over short and long time scales. The time constant τ should increase over time because of stress relaxation if the rheology is nonlinear. This is consistent with several geodetic observations [*Savage and Svarc*, 1997; *Nishimura et al.*, 2000; *Segall et al.*, 2000; *Zweck et al.*, 2002; *Kenner and Segall*, 2000].

3. Constraints on Shear Zone Rheology From GPS Data

[32] The postseismic displacement history of a shear zone produces a GPS signal, which ideally can be inverted to constrain the shear zone rheology. However, several complications related to model assumptions, heterogeneity of the displacement history, and noise in the GPS data, limit the resolution of stress exponent estimates. In particular, the assumption that tectonic loading can be neglected, necessary to derive the analytical general relaxation law, might not be valid. In this section, I present a simple method of constraining $1/n$ from a GPS record, and the trade-offs that exist with respect to model assumptions.

3.1. Estimation of an Apparent $1/n$ and τ From GPS Data

[33] If the displacement history of the shear zone obeys equation (11b), the GPS signal, which is linearly related to shear zone displacement, follows equation (11b) as well, albeit with modified intensity. In other words, D_0 and V_0 are modified, but $1/n$ and τ are preserved. Hence it is possible to invert the GPS signal using equation (11b) to yield an apparent value of $1/n$ and τ, which may have direct implications for the rheology of the shear zone.

[34] To constrain values of the inverse stress exponent from a deformation record, I used a Levenberg-Marquardt optimization scheme [e.g., *Press et al.*, 1992]. This algorithm uses a time series of displacement data to estimate $\{D_0, V_0, \tau, 1/n\}$ and the associated covariance matrix (Appendix A). Figure 3a shows the best fitting curve through a synthetic data set constructed with $1/n = 0.3$. The best fit has $1/n = 0.352$. This example uses 200 data points and a noise normally distributed with standard deviation of 0.2. Tests with less data points or more noise did not return a meaningful result. Even for these parameters, different noise patterns could have returned parameter fits quite different from the input values (this problem does not arise at smaller noise levels).

[35] The Levenberg-Marquardt method returns a formal estimate of the parameter uncertainty based on the jacobian of equation (11b) at the best fit point (Appendix A). There is a strong positive correlation between $1/n$ and τ. This can be visualized by scanning the $1/n$-τ space, determining at each point the best fitting D_0 and V_0 (through a linear least squares inversion) and plotting the residual for this best fit. This is done in Figure 3b for the same simulated data set as in Figure 3a. Therefore $1/n$ and τ cannot be constrained separately.

[36] The map of residuals can be used to define a 90% confidence region. This region provides a more accurate description of the uncertainty on the rheology parameters than the formal uncertainties as the noise in GPS data is colored [*Langbein and Johnson*, 1997]. The 90% confidence region is larger for greater noise level and for smaller data sets. This reduces the number of geodetic records that can be used for constraining shear zone rheology in the postseismic interval. However, the advent of continuous GPS can now provide records of sufficient quality to constrain $1/n$.

[37] The inversion routine provides an estimate of D_0, V_0, τ, and $1/n$. However, the apparent $1/n$ and τ can be meaningless if heterogeneities of the shear zone slip distribution are important. A realistic shear zone is likely to be heterogeneous, at least because of higher temperatures at depths. In addition, the stress perturbation produced by an earthquake varies with position. A better model of a shear zone may be several shear zone patches, each coupled with one another, and each producing a postseismic signal. None of these signals would be exactly given by equation (11). Even if the generalized relaxation curve is approximately valid for each patch, the rheological parameters may vary from one shear zone patch to another. A GPS signal is the

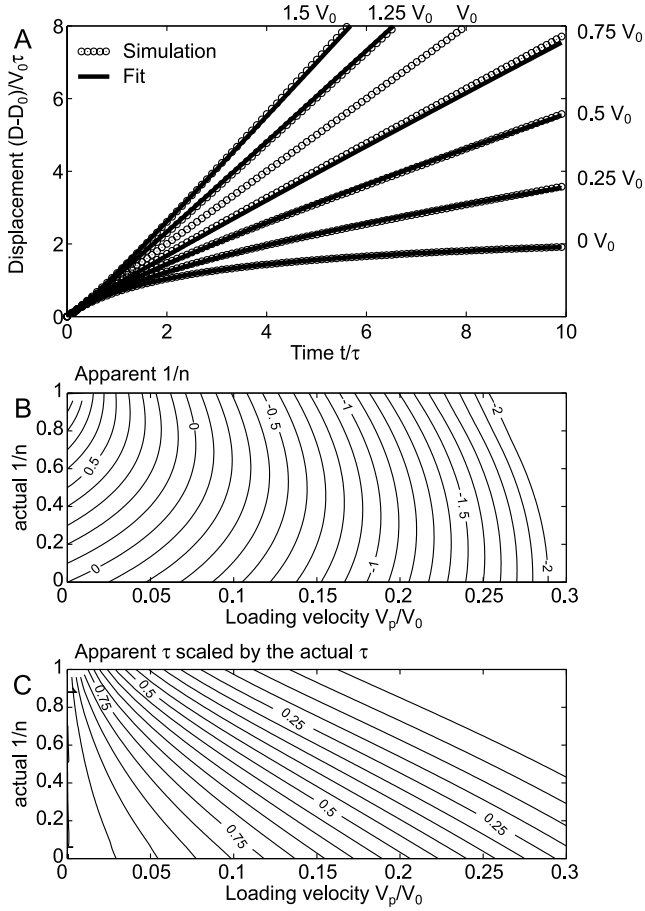

Figure 4. Effect of reloading velocity V_P on postseismic creep. (a) Simulations of postseismic creep with $n = 3$ and the reloading velocity V_P varying from 0 to 1.5 V_0. Simulation results are circles. The solid lines are the best fits obtained with equation (11) and no reloading velocity. (b) and (c) Apparent values of $1/n$ and τ obtained by fitting equation (11) to simulations with nonzero V_P. The results depend on the maximum time for the simulations, here 10τ.

convolution of the displacement history of all the shear zone patches. It may turn out very different from equation (11b).

[38] Nevertheless, heterogeneities in the displacement history of a shear zone are not necessarily a major problem because the sensitivity kernel of a GPS station is itself heterogeneous: as each station is most sensitive to a limited area of the shear zone, each GPS record produces an estimate of $1/n$ and τ in the region of maximum sensitivity. Varying τ and $1/n$ estimates across a GPS network may reflect the different displacement histories of various shear zone patches. For instance, stations closer to the fault trace would be sensitive to shallower levels, where the strength of the shear zone and τ may be higher. However, constraining these variations is made difficult by the correlation between the various inversion parameters.

3.2. Effect of Reloading Velocity

[39] The inversion routine described above provides an estimate of $1/n$ and τ, which characterize the rheology of a shear zone. These estimates assume that equation (11) is valid, i.e., that the loading velocity V_P can be neglected in the postseismic interval. This assumption is not strictly true. *Marone et al.* [1991] handles this problem for the frictional case by simply adding V_P to the shear zone velocity V_S. However, this is strictly valid only if the rheology is linear. In all other cases, V_P must be included in equation (4). If the shear zone rheology is similar to velocity-strengthening friction (equation (1)), the displacement and slip history is given by

$$\frac{V_S}{V_0} = \left[\left(1 + \frac{V_0}{V_P}\right)\exp\left(\frac{V_P}{V_0}\frac{t}{\tau}\right) - \frac{V_0}{V_P}\right], \tag{15}$$

$$\frac{D_S - D_0}{V_0\tau} = \log\left\{1 + \frac{V_0}{V_p}\left[1 - \exp\left(-\frac{V_P}{V_0}\frac{t}{\tau}\right)\right]\right\}. \tag{16}$$

In all other cases, the velocity history cannot be solved analytically. I resort then to numerical methods.

[40] Figure 4a shows the displacement history of a shear zone with $n = 3$ reloaded at different values of V_P. In each case, the displacement history can be matched well with equation (11), albeit with a different $1/n$ and τ than the actual value. The apparent $1/n$ and τ decrease with increasing V_P/V_0 (Table 2 and Figures 4b and 4c). Negative values of apparent $1/n$ appear when V_P cannot be neglected. For $V_P > V_0/2$, the inversion scheme returns imaginary values of $1/n$, revealing that equation (11) loses its usefulness. When $V_P = V_0$, the shear zone is in steady state. Then, the displacement increases linearly with time, which cannot be matched with equation (11). Finally, if $V_P > V_0$, values of $1/n$ greatly in excess of 1 appear. The case occurs if the earthquake reduces the stress on the aseismic region where postseismic creep occurs. Usually, the opposite happens: stress is increased in that region, resulting in $V_0 > V_P$.

[41] In summary, reloading affects the displacement history of the shear zone. The apparent value of $1/n$ is reduced by reloading effects. Therefore the apparent $1/n$ that fits a GPS record must be considered only as a minimum estimate for the actual rheological parameter. In particular, $1/n < 0$ almost certainly indicates that reloading has influenced the displacement history of shear zone.

[42] It is possible to invert for V_P in the same time as the rheological parameters τ and $1/n$. For that purpose, I use a grid search technique in the three-dimensional parameter space $1/n$-τ-V_P/V_0. At each grid point, the remaining parameters, D_0 and V_0, are determined by linear least squares inversion. This inversion routine returns the correct parameters if there is no noise in the data. However, any level of noise that is comparable to that of GPS records prevents an accurate determination of the three major

Table 2. Apparent Values of Inverse Stress Exponent $1/n$ and Time Constant τ for Simulation With Nonzero Reloading Velocity V_P

V_P/V_0	$1/n$	τ
0	0.35	1.03
0.25	−1.6	0.155
0.5	−5.5	0.0073
0.75	imaginary	imaginary
1	$\pm\infty$	$\pm\infty$
1.25	40	1.13
1.5	27	1.02

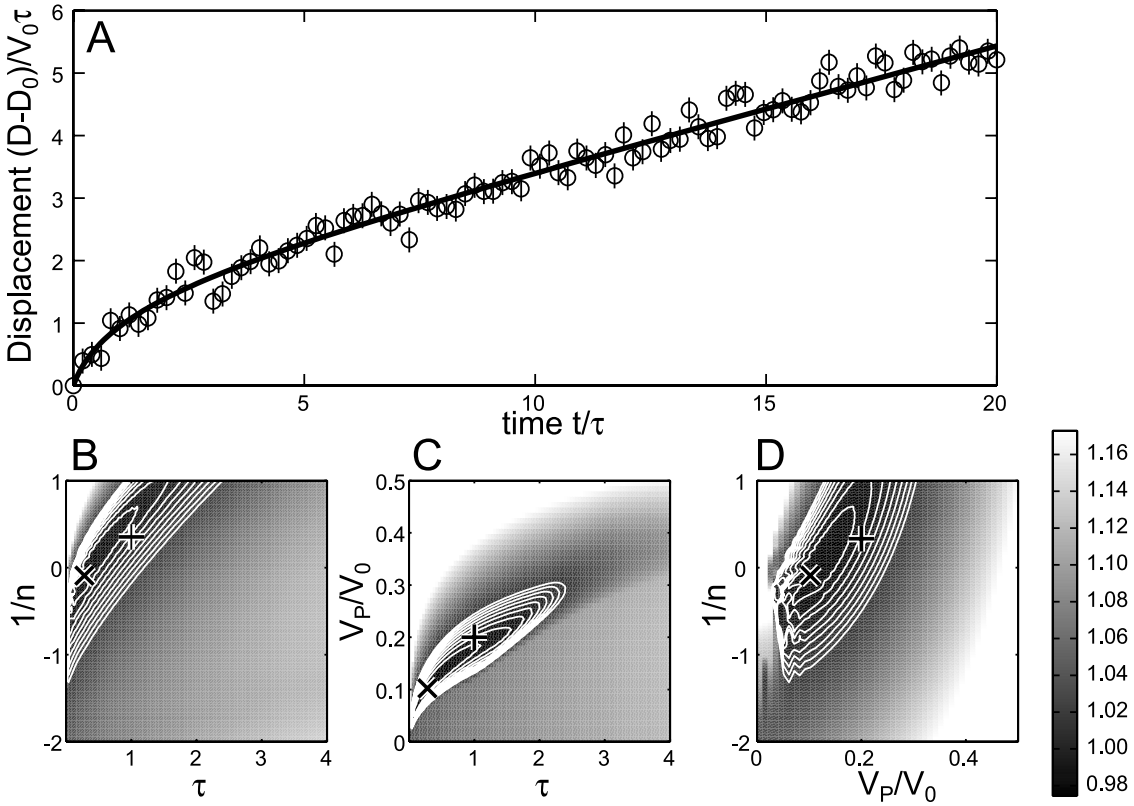

Figure 5. Inversion results for a simulated postseismic history with $1/n = 1/3$, $D_0 = 0$, $V_0 = 1$, $\tau = 1$, $V_P/V_0 = 0.2$, and random noise following a normal distribution with standard deviation of 0.2. (a) Simulated data set (circles with error bars) and the best fit obtained by the grid search method. Least misfit obtained for test values of (b) $1/n$ and τ, (c) V_P/V_0 and τ, (d) V_P/V_0 and $1/n$. Best fit is marked by the cross, and the original value is marked by the plus. In presence of noise, it is not possible to recover accurately all the original parameters.

parameters. The region of minimum misfit degenerates into a swath of low misfit values, with a strong correlation between $1/n$, τ, and V_P/V_0 (Figure 5). There is no systematic relation between the inversion result and the original parameters with even modest noise levels. In consequence, inverting for V_P/V_0 as well as $1/n$ and τ presents no advantage with respect to using the general relaxation curve.

[43] In summary, tectonic loading can have an major influence on postseismic deformation history and on the apparent values of $1/n$ and τ obtained by fitting the general relaxation law (equation (11)) to postseismic records. It is not possible to provide good constraints on any of the three parameters separately with a single record. Hence I decided to concentrate on inversions that assume the general relaxation law (equation (11), $V_P = 0$). Ideally, V_P can be determined independently from this postseismic relaxation, for instance, from long-term records or plate reconstructions. The values of $1/n$ and τ determined from individual GPS records using the general relaxation law constitute only lower bounds for the actual rheological parameters. In particular, a negative $1/n$ is probably the result of tectonic loading rather than a feature of the shear zone rheology.

4. Application to Recent Earthquakes

[44] In this section, I consider a few records collected in the aftermath of three subduction zone earthquakes and one strike-slip event and present the apparent values of $1/n$ that best fit the records. The interpretation of these results is conducted in section 5.

[45] The initial velocity V_0 reflects the earthquake-induced stress perturbation. Hence it should be different for motion observed in different directions. In general, the characteristic timescale, τ, depends on V_0. Therefore the generalized relaxation law is strictly valid only for a principal directions of motion; the observed signal in any other directions is the sum of two time decay functions similar to equation (11). Constraining τ requires that motion is first projected in a principal direction of motion. Similarly, the apparent value of $1/n$, which reflects not only the rheology, but also the intensity of reloading, is best defined along a principal direction of motion.

[46] For the records presented below, displacement occurs principally along a certain azimuth, which defines the principal component of motion. Motion perpendicular to that azimuth does not exhibit systematic trends. Hence I analyze only the time series projected along that special azimuth, determined by a linear fit through the trajectory of the station in an horizontal plane. Vertical motion, being more noisy than horizontal motion, is ignored in this analysis. The inversion results are gathered in Table 3, and their associated covariance matrices are presented in Table 4. However, the uncertainties on

Table 3. Record Information and Parameters of the Best Fitting General Relaxation Law for the Time Series in Figures 6–11

Earthquake	Station	Projection Direction	Record Duration	Amplitude, cm	D_0, cm	V_0, cm/d	τ, days	$1/n$
Peru[a]	AREQUIPA[b]	N65°E	6 July 2001 to 20 Oct. 2001	6.2	−0.52 ± 0.01	−5.7 ± 49.1	0.024 ± 0.327	−0.59 ± 0.13
Sanriku	KUJI[c]	N100°E	28 Dec. 1994 to 16 April 1996	6.4	0.22 ± 0.06	−0.062 ± 0.005	42 ± 7	0.11 ± 0.07
Sanriku	AOMORI[c]	N106°E	28 Dec. 1994 to 16 April 1996	4.7	0.14 ± 0.03	0.039 ± 0.002	41 ± 18	−0.26 ± 0.13
Sanriku	MUTSU[c]	N110°E	128 Dec. 1994 to 16 April 1996	3.7	1.65 ± 0.03	0.022 ± 0.002	95 ± 18	0.16 ± 0.13
Sanriku[d]	KUJI[b]	N80°E	28 Dec. 1994 to 6 Jan. 1995	2.3	−0.16 ± 0.39	−2.3 ± 2.5	0.40 ± 0.72	0.19 ± 0.47
Kronotsky	inversion[e]		5 Dec. 1997 to 29 Jan. 1998	188	−4.3 ± 20	49 ± 73	0.60 ± 1.6	−0.30 ± 0.38
İzmit	DUMT[f]	N57°E	17 Aug. 1999 to 11 Nov. 1999	3.2	0.02 ± 0.25	−2.2 ± 6.5	0.067 ± 0.33	−0.45 ± 0.19
İzmit	HAMT[f]	N41°E	20 Aug. 1999 to 11 Nov. 1999	3.2	−0.04 ± 0.26	−4.3 ± 50.0	0.010 ± 0.20	−0.69 ± 0.29
İzmit	KANT[f]	N65°W	17 Aug. 1999 to 11 Nov. 1999	2.3	−0.08 ± 0.11	−0.9 ± 20.8	0.008 ± 0.44	−1.53 ± 0.32
İzmit	MURT[f]	N51°E	17 Aug. 1999 to 11 Nov. 1999	5.0	0.00 ± 0.35	−3.8 ± 21.5	0.025 ± 0.26	−0.71 ± 0.21
İzmit	TUBI[f]	N71W	17 Aug. 1999 to 11 Nov. 1999	3.5	0.01 ± 0.14	−1.8 ± 5.3	0.041 ± 0.23	−0.77 ± 0.13
İzmit	UCGT[f]	N73°W	17 Aug. 1999 to 11 Nov. 1999	6.4	0.02 ± 0.16	−1.5 ± 1.3	0.199 ± 0.35	−0.73 ± 0.08

[a]Only after aftershock.
[b]*Melbourne et al.* [2002].
[c]*Heki et al.* [1997].
[d]Only before aftershock.
[e]*Bürgmann et al.* [2001].
[f]*Ergintav et al.* [2002].

each result are better characterized by the 90% confident envelope.

4.1. The 2001 Peru Earthquake

[47] The 23 June 2001 M_w = 8.4 Peru earthquake ruptured the interface between the subducting Nazca plate and south America over a 320 km ×100 km area [*Giovanni et al.*, 2002]. Notable for having released the highest moment in the previous 30 years, it produced 50 cm of coseismic displacement of the Arequipa permanent GPS station in Peru, located about 175 km east of the epicenter (Figure 6a). The station continued its southwesterly motion in the postseismic period, moving by almost another 10 cm in the next hundred days. A M_w = 7.5 aftershock occurred on 7 July 2001, which produced a sudden displacement at the GPS station [*Melbourne et al.*, 2002]. Because this aftershock is powerful enough to alter the state of stress of the crust, it is important to analyze separately the time intervals before and after the aftershock.

[48] The rate of postseismic creep decreases over time, making it possible to fit equation (11b) to the GPS time series. For that purpose, I use the 2 hours solutions of *Melbourne et al.* [2002], which have formal errors of 0.7 and 0.9 cm in the north and east directions, respectively. The signal in the vertical direction is too subtle to give meaningful estimates of apparent stress exponent.

[49] Only the portion of the time series that follows the 7 July 2001, aftershock could be fit with a reasonable degree of confidence. This is due to the short time span available between the main shock and aftershock. Following the aftershock, motion is dominantly in the N65°E direction, close to the main shock slip vector. The time decay of the displacement history is best fit with $1/n \sim -0.6$ and a very small τ (Figure 6b). However, the 90% confidence region indicates that the value of τ

Table 4. Covariance Matrices of Inversion Results

Earthquake	Record	D_0, D_0, cm^2	D_0, V_0, cm^2 yr^{-1}	D_0, τ, cm yr^{-1}	D_0, $1/n$, cm	V_0, V_0, cm^2 yr^{-2}	V_0, τ, cm	V_0, $1/n$, cm yr^{-1}	τ, τ, yr^2	τ, $1/n$, years	$1/n$, $1/n$
Peru[a]	AREQUIPA[b]	0.94	−45.7	−0.30	−0.036	2400	16	3.4	0.11	0.023	0.016
Sanriku	KUJI[c]	0.0036	−0.00025	0.32	0.0024	0.000023	−0.032	−0.00028	47	0.43	0.0043
Sanriku	AOMORI[c]	0.0027	−0.00021	0.49	0.0037	0.000020	−0.052	−0.00046	140	1.3	0.013
Sanriku	MUTSU[c]	0.0010	−0.000042	0.43	0.0026	0.0000024	−0.028	−0.00018	340	2.4	0.018
Sanriku[d]	KUJI[b]	0.15	−0.88	0.23	0.11	6.3	−1.8	−1.0	0.52	0.32	0.22
Kronotsky	slip inversion[e]	390	−1100	21	2.1	5400	−120	−22	2.67	0.55	0.14
İzmit	DUMT[f]	0.065	−1.1	−0.051	−0.0042	43	2.1	0.93	0.11	0.050	0.036
İzmit	HAMT[f]	0.067	−7.4	−0.028	−0.021	2500	9.9	12	0.040	0.049	0.087
İzmit	KANT[f]	0.012	−1.8	−0.038	−0.0024	430	9.3	4.28	0.20	0.094	0.10
İzmit	MURT[f]	0.12	−5.4	−0.062	−0.0044	460	5.6	3.1	0.067	0.039	0.041
İzmit	TUBI[f]	0.020	−0.56	−0.023	−0.0016	29	1.2	0.48	0.052	0.022	0.022
İzmit	UCGT[f]	0.026	−0.17	−0.042	−0.0029	1.8	0.46	0.079	0.12	0.022	0.0069

[a]Only after aftershock.
[b]*Melbourne et al.* [2002].
[c]*Heki et al.* [1997].
[d]Only before aftershock.
[e]*Bürgmann et al.* [2001].
[f]*Ergintav et al.* [2002].

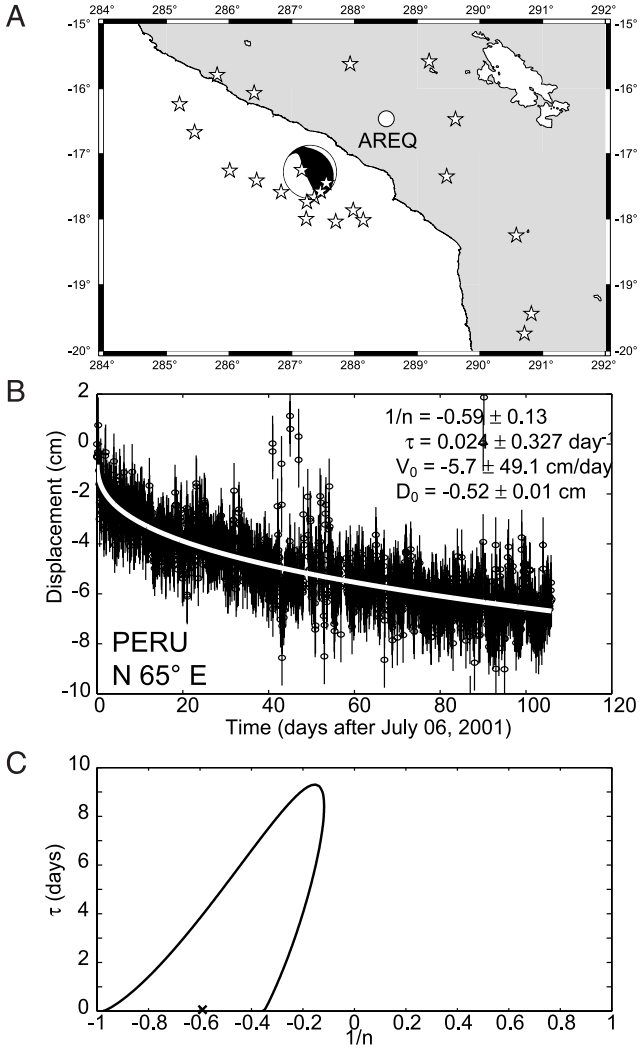

Figure 6. (a) Location map for the 2001 Peru earthquake (focal mechanism from Harvard GMT catalog), Arequipa (AREQ) GPS station (circle), and the earthquakes of $M_w >$ 4.0 in the 100 days following the main shock (stars, from the Harvard CMT catalog); (b) displacement of GPS station Arequipa (AREQ) after the 7 July 2001 aftershock along azimuth N65E (data from *Melbourne et al.* [2002]) and best fitting decay trends (solid line); and (c) 90% confidence regions for the inversion parameters fitting the time series. The cross marks the best fit.

is poorly constrained but that $1/n$ is definitively negative (Figure 6c).

4.2. The 1994 Sanriku Earthquake

[50] Like the Peru event, the 28 December 1994 M_w = 7.7 Sanriku earthquake ruptured a subduction interface, this time between the Pacific and Eurasian plates at the Japan trench. It induced postseismic displacements of several cm at several inland stations in northern Japan [*Heki et al.*, 1997; *Nishimura et al.*, 2000]. Postseismic deformation was also documented using repeating earthquakes, which allowed *Uchida et al.* [2003] to constrain that most (although not all) of the afterslip occurred in the downward continuation of the seismogenic rupture. *Nishimura et al.* [2000] identify a short-term (over a few days) and a long-term (over a year) trend in GPS data. Their short term displacement rate decays rapidly with time, whereas the long term displacement increases linearly with time. The short-term displacement is located mainly within the coseismic rupture area. The long-term displacement reveals an additional slipping patch to the south of the rupture area, with motion opposite to the coseismic motion. This is interpreted as back slip due to locked segment of the slab interface [*Nishimura et al.*, 2000]. The long-term displacement is also observed to propagate toward the south and toward the west over the year that follows the earthquake. Hence postseismic creep is generated in part in the region down dip from the rupture area, where rock behavior is dominantly aseismic [*Nishimura et al.*, 2000]. This justifies considering the generalized relaxation law of this paper to model the observed postseismic displacement, especially at long term.

[51] I inverted three time series from stations KUJI, AOMORI and MUTSU, each almost 500 days long, provided by K. Heki (personal communication, 2003). These times series are the continuation of the data presented by *Heki et al.* [1997]. These time series give $1/n = 0.11 \pm 0.07$, $1/n = -0.26 \pm 0.13$, and $1/n = 0.16 \pm 0.13$, respectively (Figure 7). All three records can be matched with $1/n \sim -0.0$, although the record from KUJI requires shorter τ at equal $1/n$ (Figure 8). Inversions of data restricted to shorter time intervals failed to show any time variation in the inferred $1/n$ and τ, within the error bars on these parameters.

[52] While the data from *Heki et al.* [1997] are a daily network solution, *Melbourne et al.* [2002] present a 2-hour solution for station KUJI. The variability inherent in this finer time resolution produces a higher noise level than in the daily solution. Hence it has proven impossible to fit the record with equation (11b) over a long time interval. A large aftershock occurred 10 days after the main shock. The 2-hour solutions provide enough data that $1/n$ could be constrained to 0.19 ± 0.47 over the first 10 days following the earthquake (Figure 9). It is encouraging that this value is consistent with the long-term inference from daily solutions at the same station. The inferred τ is much smaller than inferred from the longer-duration records in Figure 7, but its value is largely unconstrained.

4.3. The 1997 Kronostky Earthquake

[53] The final subduction zone event that I consider here is the 5 December 1997 M_w = 7.8 Kronotski earthquake. This event ruptured the interface between the Pacific and Eurasia plates offshore Kamchatka. Postseismic creep was recorded by a network of permanent GPS stations on the peninsula [*Bürgmann et al.*, 2001].

[54] In sections 4.1 and 4.2, I was fitting GPS records directly with equation (11b). However, GPS stations record only indirectly the displacement of a ductile shear zone. When a GPS network is present, it is possible to invert station displacement for the slip history of a presupposed plane. This was done for the Kamchatka event by *Bürgmann et al.* [2001]. Hence the generalized relaxation law can be applied directly to the slip history of the aseismically creeping shear zone.

[55] The shear zone that provides the best fit to the postseismic creep time series is located near the bottom edge of the coseismic fault plane and extends beyond the coseismic fault plane [*Bürgmann et al.*, 2001]. The slip rate on this shear zone decreases over time, which again indicates the equation (11) is reasonable. I fitted the general relaxation law to the smoothed version of the afterslip history (Figure 10). This gives $1/n = -0.30 \pm 0.38$. However, the correlation between $1/n$ and τ estimates allows values of $1/n$ as high as 0.8, provided that τ is increased to 19 days.

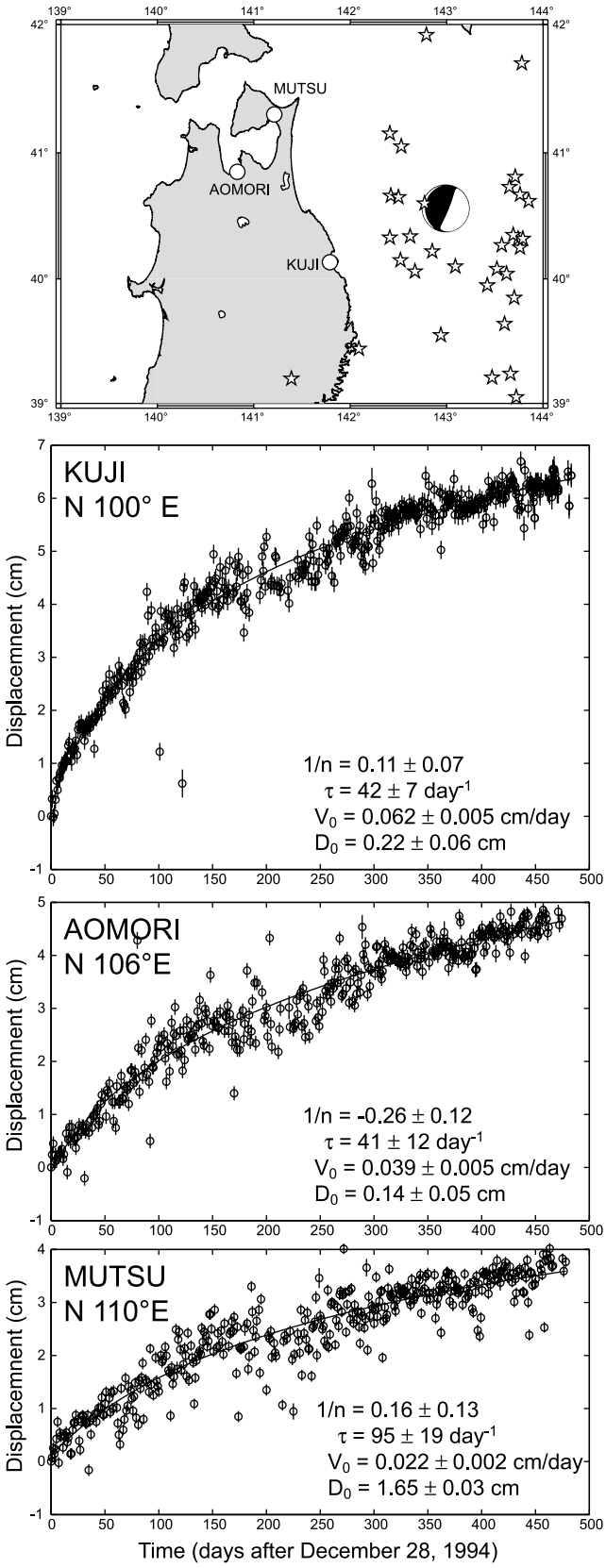

Figure 7. Time series of eastward displacement of GPS station KUJI (projected N110°E), AOMORI (projected N106°E), and MUTSU (projected N110°E), in Japan, following the 1994 Sanriku earthquakes (data from *Heki et al.* [1997]). The best fitting decay trends are shown with the solid line. Inversion results are shown on each graph. (top) Location of the three stations (circles), the earthquake (focal mechanism from Harvard GMT catalogue), and all the earthquakes of $M_w > 4.0$ in the 500 days following the Sanriku earthquake in the Harvard CMT catalogue (stars).

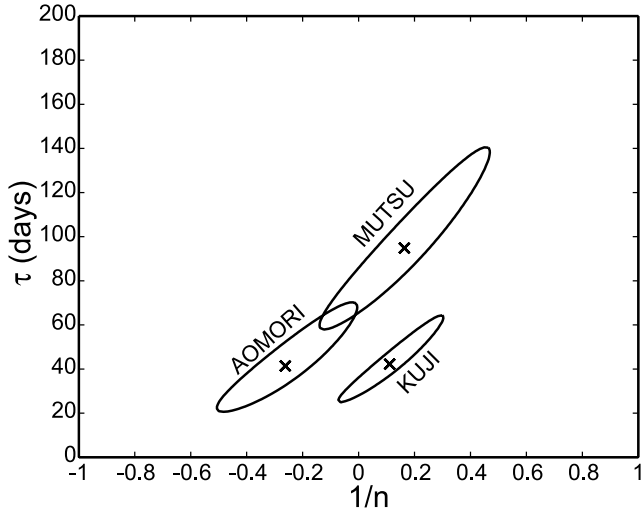

Figure 8. The 90% confidence regions for the inversion parameters fitting the time series collected after the 1994 Sanriku presented in Figure 7. Crosses indicate the best fit.

4.4. The 1999 İzmit Earthquake

[56] The 17 August 1999 $M_w = 7.5$ İzmit earthquake was a large continental strike-slip earthquake that ruptured the North Anatolian fault over more than 100 km. It was followed 88 days later by a $M_w = 7.2$ earthquake, the 12 November 1999 Düzce earthquake. These earthquakes are part of a sequence of events that ruptured most of the North Anatolian fault in the 20th century [*Ambraseys*, 2002]. Intuitively, there is a causal relation between the two earthquakes, which must be understood if risks following a major event are to be assessed accurately. While the static stress at the Düzce epicenter was increased as a result of the İzmit earthquake, the time delay between the events can be attributed to postseismic creep [*Hearn et al.*, 2002]. In that respect the İzmit-Düzce earthquake pair resembles the Landers-Hector Mine earthquake pair [*Freed and Lin*, 2001].

[57] Postseismic creep is observed in GPS data in the time interval between the two 1999 Turkish earthquakes [*Bürgmann et al.*, 2002; *Ergintav et al.*, 2002]. Postseismic

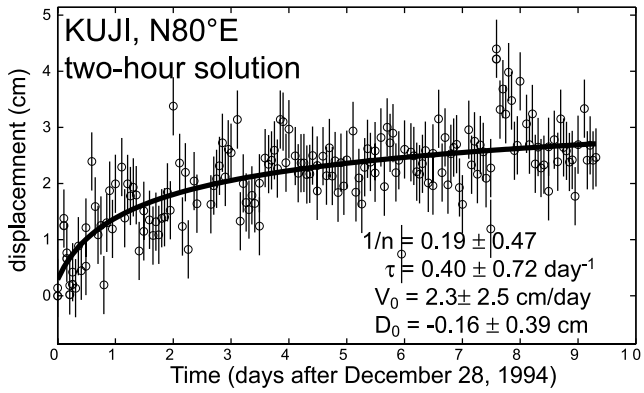

Figure 9. Two-hour solutions of displacement of GPS station KUJI following the 1994 Sanriku earthquakes projected along direction N80°E (data from *Melbourne et al.* [2002]). The best fitting decay trend is shown with the solid line. Inversion results are shown on the graph.

displacement is concentrated in the region below the İzmit rupture. Two main patches can be identified in the inversion of GPS data: a relatively shallow patch active during the first 30 days, and a deeper patch located near the eastern end of the rupture, active for the entire time interval separating the two earthquakes [*Bürgmann et al.*, 2002]. These two centers may complicate the application of the general relaxation law. Because of their separation, there may be a systematic difference between the rheology apparent at GPS stations close to the epicenter and more easterly stations, the former being sensitive to the first patch and a frictional rheology ($1/n \sim 0$) and the latter to the second patch and a ductile rheology ($1/n \sim 0.3$).

[58] I fitted the general relaxation law (equation (11)) to the continuous GPS time series collected at 20 stations between the İzmit and Düzce earthquakes [*Ergintav et al.*, 2002] provided by S. McClusky (personal communication, 2003). Each record was projected in the direction of principal motion, as describe above (Table 3). Of these 20 records, 6 provide reasonable constraints on the rheological parameters entering the general relaxation law (Figure 11). The inversion results are gathered in Table 3. The others have either too small amplitude or display a linear trend that cannot reflect a relaxation process. Formal uncertainties allow negative values for the τ parameter in all these cases, but in fact, the confidence regions reject such values (Figure 12).

[59] All the records except KANT are compatible with $1/n \sim -0.7$ and τ less than a few days. The agreement between stations HAMT, MURT, TUBI, and UCGT is particularly impressive, UCGT and TUBI being the best constrained records. The record from station DUMT hints at higher values of $1/n$, but the difference with UCGT is not significant at the 90% confidence level. With the caveat that it is the least constrained of the records that I retain here, KANT requires more negative $1/n$ values. KANT is also much further from the fault than the other stations (Figure 11).

5. Discussion

[60] The analyses of geodetic data presented above yield relatively well-constrained estimates of the apparent inverse stress exponent. There appears to be no significant difference between the values of $1/n$ for subduction zone earthquakes and for the only strike-slip event studied herein, the İzmit earthquake, although this might reflect more the limits of this analysis than actually physical processes. The rheological parameters from the Kronostsky event, for which I used an estimate of shear zone displacement, not a direct GPS record, are comparable to those obtained for other events using continuous GPS data, indicating that the assumption that the time dependence of postseismic creep is preserved in GPS data is reasonable.

[61] In every case for which $1/n$ is well constrained, $1/n$ is less than 1, which indicates a nonlinear behavior. Hence diffusion creep is probably not the dominant rheology of aseismic shear zones. This agrees with the results of *Freed and Bürgmann* [2004], who model geodetic deformation following the Landers-Hector Mine earthquake pair and find it necessary to include a power law behavior in the upper mantle. The records collected after the Sanriku earthquake indicate $1/n \sim 0.0$, which may reflect velocity-strengthening friction. However, any rheological inferences must be met at this point with caution because of the trade-off with tectonic reloading. All the other GPS data imply negative $1/n$.

[62] Negative values of $1/n$ are not directly compatible with any plausible rheology for a ductile shear zone. They imply instead that one of our assumptions made in deriving equation (11) is invalid for these records. These assumptions are that (1) the reloading velocity can be neglected and (2) the signal is dominated by slip on one patch or the slip on all patches has the same time dependence. The general relaxation law does provide a good description of the time dependence of postseismic creep, but its physical meaning becomes ambiguous. In the following, I first address the importance of reloading, its implication for shear zone rheology and stress magnitude, and then whether spatial variations of physical properties can be constrained from these records.

5.1. Magnitude of Reloading and Shear Zone Rheology

[63] Tectonic loading was shown in section 3.2 to affect the time dependence of postseismic creep. In the presence of

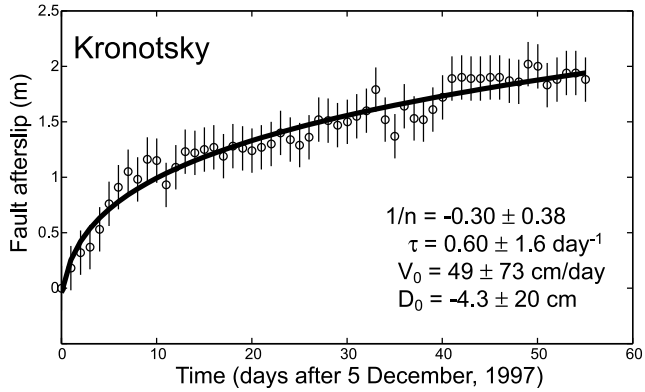

Figure 10. Estimates of fault afterslip following the 1997 Kronostsky earthquake [*Bürgmann et al.*, 2001]. The best fitting decay trends is shown with the solid line. Inversion results are shown on the graph.

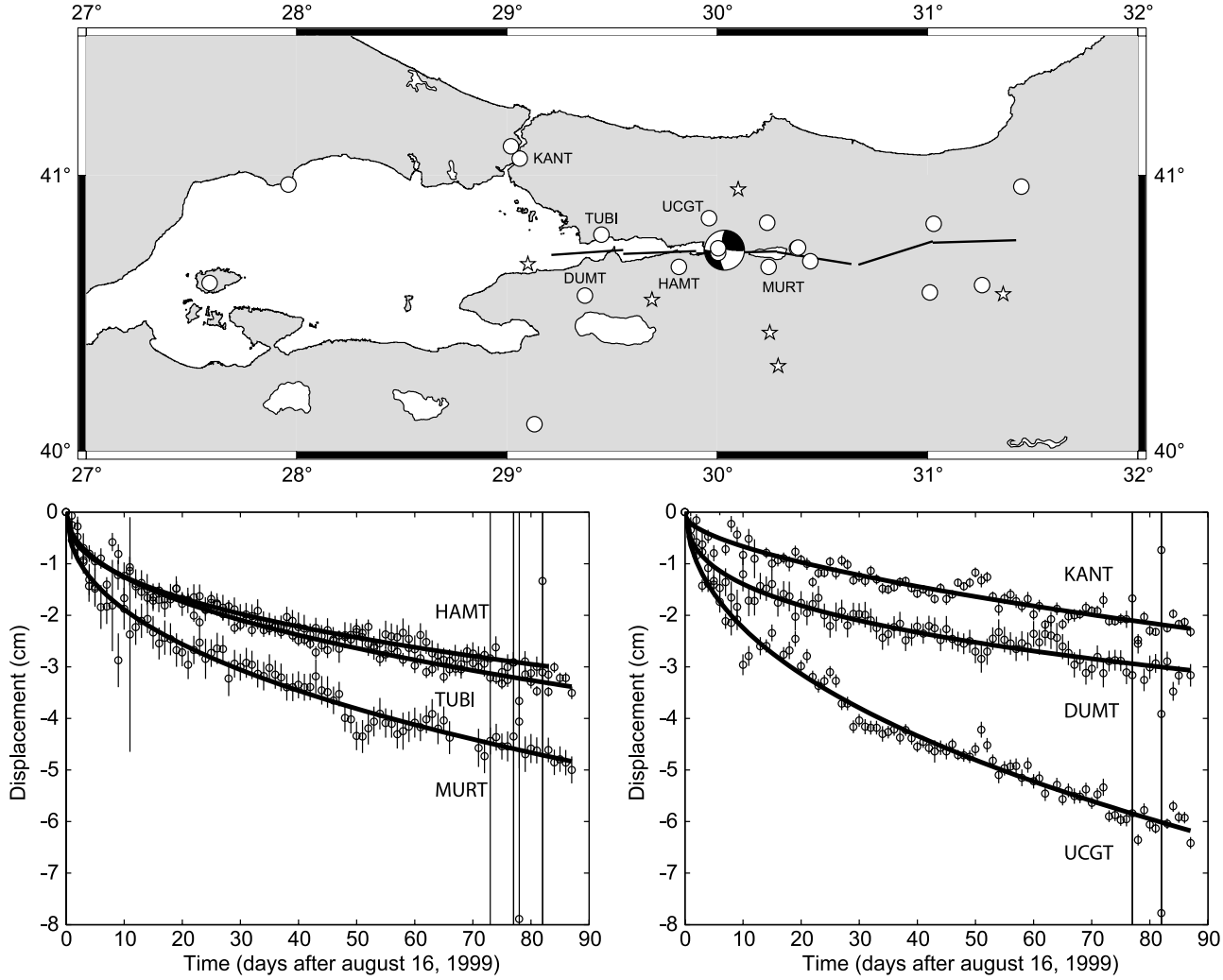

Figure 11. (top) Map of permanent GPS stations (circles) recording postseismic creep after the 1999 İzmit earthquake. Focal mechanism is of the earthquake. Stars denotes earthquake in the Harvard CMT catalogue occurring in the region between the İzmit and Düzce earthquakes. (bottom) GPS time series (circles with error bars) for which the parameters entering the general relaxation law are relatively well constrained. The fits are shown in the solid line and are compiled in Table 3. Data provided by S. McClusky, after *Ergintav et al.* [2002].

reloading, the relaxation curve implies a lower apparent $1/n$ than mandated by the rheology. This offers an appealing explanation for the negative stress exponent values implied by many of the GPS records considered in this study whereby the actual $1/n$ is positive but tectonic loading in the postseismic interval results in a negative apparent stress exponent.

[64] Reloading is quantified by the ratio of shear zone velocity due to tectonic reloading to shear zone velocity at the beginning of the record, V_P/V_0. For the best constrained records it is possible to evaluate the value of V_P/V_0 for which the misfit with the data is minimized at a given $1/n$ (Figure 13, left).

[65] For the İzmit earthquake, the reloading intensity is estimated to be less than 0.15. The shear zone velocity immediately after the earthquake reaches about 1 m/yr at depth near the epicenter [*Bürgmann et al.*, 2001]. This implies a reloading rate of at most 15 cm/yr. For comparison, the long-term slip rate of the fault is about 2.5 cm/yr [*Ambraseys*, 2002; *Meade et al.*, 2002]. In the simple model used in this study, there is no mechanism for the reloading rate to exceed the long-term shear zone velocity. Using $V_P \sim 2.5$ cm/yr and $V_0 \sim 100$ cm/yr implies values of $1/n$ near 0 (Figure 13). This may indicate that velocity-strengthening friction is responsible for postseismic creep, in agreement with *Hearn et al.* [2002]. However, considering the uncertainties of this analysis, it is premature to consider this conclusion definitive.

[66] Postseismic creep following the 2001 Peru and 1997 Kronotsky earthquakes also indicates negative stress exponents, which can be interpreted as an actually positive stress exponent with V_P/V_0 of order 0.05–0.2. At the location of the Kronotsky event, the Pacific plate plunges underneath Kamchatcka at roughly 6 cm/yr. Fitting the postseismic creep gives $V_0 \sim 180$ m/yr, about a factor of 3000 faster than the plate convergence rate. This would imply that

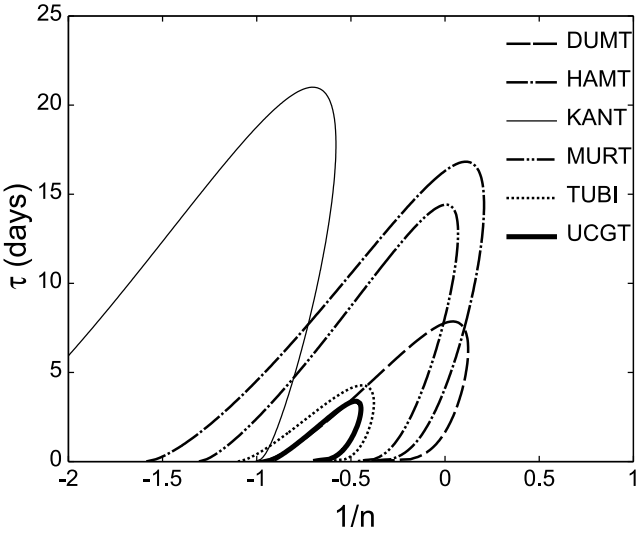

Figure 12. The 90% confidence regions for the inversion parameters fitting the time series collected after the 1999 İzmit earthquake presented in Figure 11.

V_P/V_0 is actually very small for this event, and that reloading cannot explain the negative apparent stress exponent. In this case, it may be that the deformation mechanism of the shear zone is different from those considered in this study. However, the uncertainties in this analysis again prevent a definitive conclusion to be reached: if $1/n$ is less than 0.5, there is no minimum estimate of V_P/V_0 in the 90% confidence interval (Figure 13).

[67] Creep following the 1994 Sanriku earthquake does not require reloading. The records point consistently toward $1/n$ of order 0.0 if reloading is ignored (Figure 8). The records from the KUJI station show a good agreement between the long-term and short-term data, although the uncertainty on $1/n$ from short-term data is rather large. Even the record from station AOMORI, for which the best fitting $1/n$ is -0.26, is compatible with $1/n \sim 0.0$ within uncertainty. Nevertheless, reloading is shown to be important for other records and may affect the Sanriku data as well. For the record of post-Sanriku deformation at KUJI, the best V_P/V_0 varies from 0 if $1/n = 0.11$ to 0.1 if $1/n = 1$. In summary, ignoring reloading, velocity-strengthening friction can explain all the records. However, as reloading seems important in other records, it is doubtful that it should be ignored here. From the KUJI record, the actual shear zone rheology is likely to have $1/n \geq 0.1$, indicative of ductile creep such as dislocation creep.

5.2. Stress Magnitude

[68] Assuming a value for the actual $1/n$, the best fitting value of V_P/V_0 can be transformed into an estimate of the ratio of earthquake-induced stress change on the shear zone, σ_E, scaled by the stress required for steady state creep at the tectonic loading rate, σ_P. Assuming a power law rheology (equation (2)), this gives

$$\sigma_E/\sigma_P = (V_P/V_0)^{-1/n} - 1. \quad (17)$$

Estimates of σ_E/σ_P for the KUJI, DUMT, TUBI, UCGT, and Kronotsky records are reported in Figure 13 (right), as a function of the assumed $1/n$. Equation (17) is not valid in the limit $1/n \rightarrow 0$, where material is inferred to obey a velocity-strengthening friction law (equation (1)). For a frictional rheology, converting the velocity ratio into a stress ratio requires imposing a value on the rheological parameter C.

[69] The estimates in Figure 13 show that earthquake-induced stress changes are important compared to the background stress applied on the presupposed shear zone imposed by tectonic loading. This is particularly true if the shear zone rheology is actually Newtonian ($1/n = 1$). Newtonian rheologies are particularly relevant for ductile shear zones because the observed reduction in grain size tends to favor diffusion creep and the presence of fluids facilitates pressure solution creep, both of which produce Newtonian behavior [e.g., *Evans and Kohlstedt*, 1995].

[70] The quantity σ_E corresponds to the coseismic Coulomb stress change at the location of the shear zone, with magnitude of a few MPa [*Harris*, 1998; *Stein*, 1999; *Hearn et al.*, 2002; *Montési*, 2004]. It may be used as a stress scale to estimate the stress supported by the shear zone at the rate of tectonic loading, σ_P. The possibly large values of σ_E/σ_P coming from this study imply that shear zones must be rather weak, with $\sigma_P \sim 1$ MPa. For power law creep with $1/n > 0.2$, as expected for ductile deformation mechanisms in rocks, the background stress is of the same order of magnitude as σ_E.

[71] Such low stresses probably indicate a structural or thermal heterogeneity in the aseismic lithosphere, a weak shear zone. *Montési* [2004] provides a lengthier discussion of shear zone strength and how the implied ratios σ_E/σ_P are difficult to reconcile with laboratory-determined flow laws. Field observations have long documented that ductile shear zones are associated with structural changes such as a reduced grain size or the presence of hydrous minerals that produce a rock that is intrinsically weaker than its surroundings.

[72] Nevertheless, stresses of several hundreds MPa have been inferred from the microstructure of several shear zones [e.g., *Küster and Stöckhert*, 1999; *Trepmann and Stöckhert*, 2003]. Such high stresses record transient phenomena that may be earthquake related. High stresses may occur at the beginning of shear zone formation while structural damage is being forced on the rock. Alternatively, high stresses are expected over a limited depth range in the vicinity of the

Figure 13. (left) Intensity of reloading for which the best fit can be achieved assuming a value of $1/n$ between 0 and 1. (right) Values of V_P/V_0 which are converted into the ratio of earthquake-induced stress change, σ_E, over the stress on the shear zone at the rate of tectonic loading, σ_P. Thick lines show the best fitting values of V_P/V_0 and σ_e/σ_P and the thin lines the 90% confidence interval at a given $1/n$. Estimates obtained for the GPS records of station KUJI following the Sanriku earthquake (Figure 7), and DUMT, TUBI, and UCGT following the İzmit earthquake (Figure 11) and for the slip inversion after the Kronotsky earthquake (Figure 10).

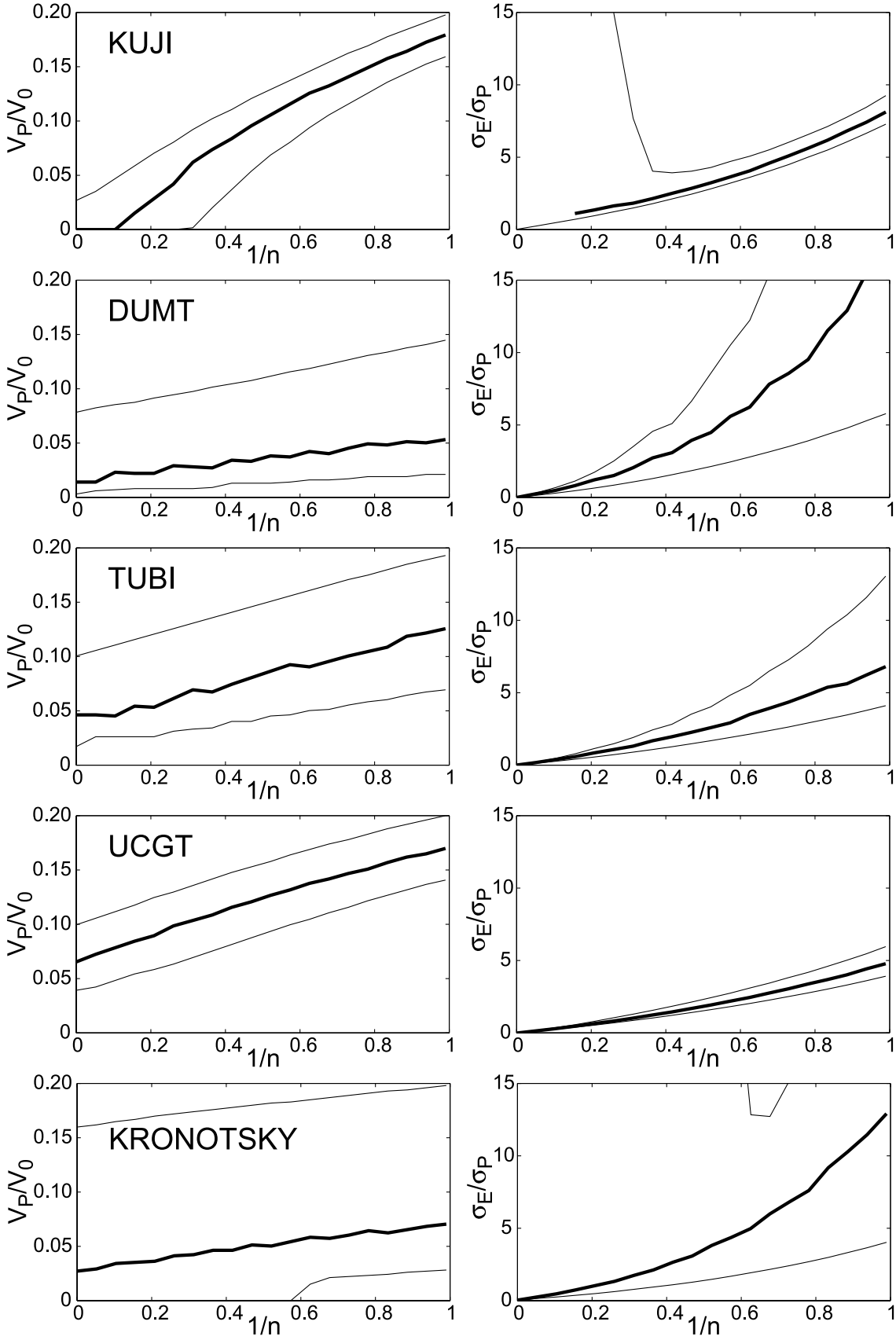
KUJI
DUMT
TUBI
UCGT
KRONOTSKY
V_P/V_0
σ_E/σ_P
1/n
0
0.05
0.10
0.15
0.20
5
10
15
0.2
0.4
0.6
0.8
1

Figure 13

seismic ruptures. A synoptic shear zone model may have a shallow high stress environment within a few km from the brittle-ductile transition followed at greater depth by a weaker region where shear zone strength is consistently lower. The high strength region may or may not be able to produce observable postseismic creep due to slip complexity but the postseismic signals discussed in this study, which require low shear zone strength, may be generated in the deeper, low strength portion of the shear zone [*Montési*, 2004].

5.3. Variations Within a Network

[73] An assumption made in this work is that spatial variations in shear zone properties are not important. Obviously, this is a gross simplification of an actual shear zone. To test this hypothesis, one must look at variations in the postseismic creep history collected at different GPS stations after a single event. Each station is sensitive to a restricted location on the shear zone. Variations of postseismic deformation within a GPS network can therefore reveal heterogeneities in shear zone behavior.

[74] The three long-term GPS records collected after the Sanriku earthquake point to a similar stress exponent, but the timescale associated with the KUJI record is slightly shorter than that deduced from the AOMORI and MUTSU records (Figure 8). KUJI is the easternmost of these three stations. It is sensitive to shallower portions of the subduction interface than MUTSU and AOMORI. Hence the Japanese data set may indicate a gradient in the strength of the plate interface with depth. The deeper levels may be weaker due to high temperatures. By contrast, the deformation mechanism does not appear to change with depth.

[75] The larger data set from the İzmit earthquake analyzed in this study has the best potential to reveal spatial variations in shear zone property. However, the analysis is limited to the 80 days separating the İzmit to the Düzce earthquakes, as for nonlinear rheologies, the combined effect of these events cannot be evaluated simply. In consequence, many of the results from the Turkish data set are rather uncertain, especially for the timescale τ. Nevertheless the agreement between stations HAMT, MURT, TUBI, and UCGT is remarkable (Figure 12). In fact, the only difference between these records seems to be in the amplitude of the signal. The four stations may be sensitive to a single slip patch with relatively uniform rheology and initial velocity. The different signal amplitude would in this case be the result of the transfer function from this patch to each station. Stations DUMT and especially KANT, located further from the fault plane near its western termination appear to differ significantly from the other four. They may be sensitive to a combination of different postseismic signals. Unfortunately, fits to the more easterly stations, which may be sensitive to a second slip patch at greater depth [*Bürgmann et al.*, 2002] were not as well constrained. This is due to shorter duration of the record in some cases and further distance from the fault in other.

6. Conclusions

[76] The rheology of aseismic shear zones influences the time dependence of postseismic creep in a predictable manner. In the absence of reloading, the response of a velocity-strengthening frictional surface and of ductile shear zones can be described by a generalized relaxation law (equation (11)) by means of an adjustable parameter, the apparent stress exponent, n. Friction is modeled with $1/n \rightarrow 0$ and viscous flow by $1/n \rightarrow 1$. Reloading of the shear zone in the postseismic time interval lowers the apparent stress exponent of the generalized relaxation law, possibly to negative numbers.

[77] The postseismic slip history observed after several recent earthquakes is adequately modeled by the generalized relaxation laws. However, a negative $1/n$ is often required by the records. This indicates that reloading cannot be neglected. The signal observed after the 1994 Sanriku earthquake provides the best constraints on shear zone rheology at this point, indicating a nonlinear rheology for this event. For the 1999 İzmit earthquake, it is seen that reloading occurs at about one tenth of the initial shear zone velocity. This implies that the magnitude of earthquake-induced stress perturbation is comparable to the shear zone strength, probably because the shear zone is weaker than the surrounding lithosphere. Hints of different behavior at different shear zone patches are provided by the Sanriku data set.

[78] Application of the relaxation law to actual postseismic records is made difficult by the covariation of inversion parameters and the unknown contribution of reloading. In addition, it is assumed that a single patch of an aseismic shear zone dominates the observed GPS signals or that all shear zone patches deform with the same time dependence. Assessment of these assumptions, as well as better constraints on shear zone rheology, requires the consideration of the complete data return by a network of continuous GPS stations after an earthquake. High-quality GPS data are being collected after recent earthquakes [e.g., *Freymueller et al.*, 2002; *Yu et al.*, 2003]. Should these records cover a longer time span than available for the İzmit earthquake, it will be possible to better address shear zone rheology using the time dependence of postseismic creep.

Appendix A: Uncertainty of the Inversion Results

[79] The parameters in equation (11b) are constrained from displacement time series using the Levenberg-Marquardt algorithm [e.g., *Press et al.*, 1992]. The measure of goodness of fit is

$$\chi^2 = \sum_{i=1}^{N} \left[\frac{D_S(t_i) - D_S(t_i, \mathbf{P})}{E_i} \right]^2, \tag{A1}$$

where i is an index for each of the N data points, t_i is the time at which data point i is collected, $D_S(t_i)$ is the measured displacement value, $D_S(t_i, \mathbf{P})$ the predicted value given a trial value $\mathbf{P}$ for the parameters in equation (11b), and E_i the uncertainty on data point i. The parameter vector $\mathbf{P}$ is defined as

$$\begin{aligned} P_1 &= D_0, \\ P_2 &= V_0, \\ P_3 &= \tau, \\ P_4 &= 1/n. \end{aligned} \tag{A2}$$

The increment of $\mathbf{P}$ is set to a value intermediate between the prediction by steepest descent and the inverse Hessian

methods. These end-member cases use the first and second derivatives of χ^2 in the four-dimensional parameter space.

[80] The uncertainty on the inversion result can be estimated from the covariance matrix $\mathbf{C} = \mathbf{A}^{-1}$, with $\mathbf{A}$ defined as one half of the Hessian (or curvature) matrix

$$A_{kl} = \frac{1}{2}\frac{\partial^2\chi^2}{\partial P_k \partial P_l} \sim \sum_{i=1}^{N} \frac{1}{E_i^2}\left[\frac{\partial D_S(t_i,\mathbf{P})}{\partial P_k}\,\frac{\partial D_S(t_i,\mathbf{P})}{\partial P_l}\right]. \quad \text{(A3)}$$

The partial derivatives in equation (A3) can be obtained analytically

$$\frac{\partial D_S(t_i,\mathbf{P})}{\partial D_0} = 1, \quad \text{(A4)}$$

$$\frac{\partial D_S(t_i,\mathbf{P})}{\partial V_0} = \frac{\tau}{1/n}\left\{1 - [1 + (1-1/n)t/\tau]^{-[1/n(1-1/n)]}\right\}, \quad \text{(A5)}$$

$$\frac{\partial D_S(t_i,\mathbf{P})}{\partial \tau} = \frac{V_0}{1/n}\left\{\begin{array}{l} 1 - (1 + t/\tau)\times \\ [1 + (1-1/n)t/\tau]^{-[1/(1-1/n)]}\end{array}\right\}, \quad \text{(A6)}$$

$$\frac{\partial D_S(t_i,\mathbf{P})}{\partial (1/n)} = nV_0\tau \cdot\left\{-n + [1 + (1-x)t/\tau]^{-\frac{1/n}{1-1/n}} \cdot\left\{n - \frac{t/\tau}{(n-1)[1 + (1-1/n)t/\tau]} + \frac{1}{(1-1/n)^2}\log\left[1 + \left(1 - \frac{1}{n}\right)\frac{t}{\tau}\right]\right\}\right\} \quad \text{(A7)}$$

The covariance matrix $\mathbf{C}$ has both diagonal and nondiagonal components. To estimate the importance of nondiagonal elements, it is convenient to scale them with the square root of the corresponding diagonal elements. For instance, C_{12} is important if $C_{12} \approx \sqrt{C_{11}C_{22}}$. Table 4 shows the magnitude of the nondiagonal elements for the inversion of geodetic data presented in this paper.

[81] Although the covariance matrix could be used to define an error ellipse, this ellipse would be only a approximation of the actual confidence region, as the errors are not normally distributed. The confidence regions in this paper are instead drawn by contouring χ^2 at a value of 7.78 above the minimum χ^2. This value is chosen to give a 90% confidence region with four degrees of freedom if the errors were normally distributed. These four degrees of freedom are D_0, V_0, τ and either $1/n$ (Figures 6c, 8, and 12) or V_p/V_0 (Figure 13).

[82] **Acknowledgments.** This work was made possible thanks the willingness of Tim Melbourne, Kosuke Heki, Roland Bürgmann, and Simon McClusky to share their data with me. I also thank Andy Freed and Roland Bürgmann for a preprint of their work. I benefited from discussions with Jeff Freymueller, Brad Hager, Greg Hirth, and Jeff McGuire and the comments from the Associate Editor, an anonymous reviewer, and Susan Ellis. This work was supported by the Postdoctoral Scholar Program at the Woods Hole Oceanographic Institution, with funding provided by the USGS, complemented by NSF grants OCE-9907244, OCE-0327588, EAR-0337678, and a grant from the Deep Ocean Exploration Institute at WHOI to Greg Hirth.

References

Ambraseys, N. (2002), The seismic activity of the Marmara sea region over the last 2000 years, *Bull. Seismol. Soc. Am.*, *92*, 1–18.

Bechor, N., P. Segall, Y.-J. Hsu, J. McGuire, and S.-B. Yu (2001), Time-depended inversion for post-seismic slip following the 1999 Chi-Chi Taiwan earthquake using GPS observation, *Eos Trans. AGU*, *82*(47), Fall Meet. Suppl., Abstract G22D-01.

Blanpied, M. L., D. A. Lockner, and J. D. Byerlee (1991), Fault stability inferred from granite sliding experiments at hydrothermal conditions, *Geophys. Res. Lett.*, *18*, 609–612.

Blanpied, M. L., C. J. Marone, D. A. Lockner, J. D. Byerlee, and D. P. King (1998), Quantitative measure of the variation in fault rheology due to fluid-rock interactions, *J. Geophys. Res.*, *103*, 9691–9712.

Brace, W. F., and J. D. Byerlee (1970), California earthquakes: Why only shallow focus?, *Science*, *168*, 1573–1575.

Brace, W. F., and D. L. Kohlstedt (1980), Limits on lithospheric stress imposed by laboratory measurements, *J. Geophys. Res.*, *85*, 6248–6252.

Bürgmann, R., P. Segall, M. Lisowski, and J. L. Svarc (1997), Postseismic strain following the Loma Prieta earthquake from repeated GPS measurements, in *The Loma prieta, California, Earthquake of October 17, 1989—Postseismic effects, aftershocks and Other Phenomena, U.S. Geol. Surv. Prof. Pap.*, 1550-D, D209–D244.

Bürgmann, R., M. G. Kogan, V. E. Levin, C. H. Scholz, R. W. King, and G. M. Steblov (2001), Rapid aseismic moment release following the 5 December, 1997 Kronotsky, Kamchatka, earthquake, *Geophys. Res. Lett.*, *28*, 1331–1334.

Bürgmann, R., S. Ergintav, P. Segall, E. H. Hearn, S. McClusky, R. E. Reilinger, H. Woith, and J. Zschau (2002), Time-dependent afterslip on and deep below the İzmit earthquake rupture, *Bull. Seismol. Soc. Am.*, *92*, 126–137.

Casarotti, E., A. Piersanti, F. P. Lucente, and E. Boschi (2001), Global postseismic stress diffusion and fault interaction at long distances, *Earth Planet. Sci. Lett.*, *191*, 75–84.

Chéry, J., S. Carretier, and J.-F. Ritz (2001), Postseismic stress transfer explains time clustering of large earthquakes in Mongolia, *Earth Planet. Sci. Lett.*, *194*, 277–286.

Deng, J., M. G. H. Kanamori, and E. Hauksson (1998), Viscoelastic flow in the lower crust after the 1992 Lander, California, earthquake, *Science*, *282*, 1689–1692.

Dieterich, J. H. (1978), Time-dependent friction and the mechanics of stick-slip, *Pure Appl. Geophys.*, *116*, 790–806.

Dieterich, J. H. (1992), Earthquake nucleation on faults with rate- and state-dependent strength, *Tectonophysics*, *322*, 115–134.

Dieterich, J. H. (1994), A constitutive law for rate of earthquake production and its application to earthquake clustering, *J. Geophys. Res.*, *99*, 2601–2618.

Donnellan, A., and G. Lyzenga (1998), GPS observations of fault afterslip and upper crustal deformation following the Northridge earthquake, *J. Geophys. Res.*, *103*, 21,285–21,297.

Ergintav, S., R. Bürgmann, S. McClusky, R. Çakmak, R. Reilinger, O. Lenk, A. Barka, and H. Özener (2002), Postseismic deformation near the İzmit earthquake (17 August 1999, *M* 7.5) rupture zone, *Bull. Seismol. Soc. Am.*, *92*, 194–207.

Evans, B., and D. L. Kohlstedt (1995), Rheology of rocks, in *Rock Physics and Phase Relations: A Handbook of Physical Constants*, *AGU Ref. Shelf*, vol. 3, edited by T. J. Ahrens, pp. 148–165, AGU, Washington, D. C.

Fitz Gerald, J. D., and H. Stünitz (1993), Deformation of granitoids at low metamorphic grade, I: Reactions and grain size reduction, *Tectonophysics*, *221*, 269–297.

Freed, A. M., and R. Bürgmann (2004), Evidence of power-law flow in the Mojave Desert mantle, *Nature*, *430*, 548–551.

Freed, A. M., and J. Lin (2001), Delayed triggering of the 1999 Hector Mine earthquake by viscoelastic stress transfer, *Nature*, *411*, 180–183.

Freed, A. M., and J. Lin (2002), Accelerated stress buildup on the southern San Andreas fault and surrounding regions caused by Mojave Desert earthquakes, *Geology*, *30*, 571–574.

Freymueller, J., R. Bürgmann, E. Calais, A. Freed, E. Price and Denali Fault GPS Field Crew (2002), An unparallel opportunity to study post-seismic processes, *Eos Trans. AGU*, *83*(47), Fall Meet. Suppl., Abstract S72F-1365.

Giovanni, M. K., S. L. Beck, and L. Wagner (2002), The June 23, 2001 Peru earthquake and the southern Peru subduction zone, *Geophys. Res. Lett.*, *29*(21), 2018, doi:10.1029/2002GL015774.

Harris, R. A. (1998), Introduction to special section: Stress shadows, and their implications for seismic hazard, *J. Geophys. Res.*, *103*, 24,347–24,358.

Hearn, E. H., R. Bürgmann, and R. E. Reilinger (2002), Dynamics of İzmit earthquake postseismic deformation and loading of the Düzce earthquake hypocenter, *Bull. Seismol. Soc. Am.*, *92*, 172–193.

Heki, K., S. Miyazaki, and H. Tsuji (1997), Silent fault slip following an interplate thrust earthquake at the Japan trench, *Nature*, *386*, 595–598.

Hirth, G., and D. L. Kohlstedt (2003), Rheology of the upper mantle and the mantle wedge: A view from the experimentalists, in *The Subduction Factory*, *Geophys. Monogr. Ser.*, vol. 138, edited by J. Eiler, pp. 83–105, AGU, Washington, D. C.

Hobbs, B. E., A. Ord, and C. Teyssier (1986), Earthquakes in the ductile regime?, *Pure Appl. Geophys.*, *124*, 309–336.

Hsu, Y., N. Bechor, P. Segall, S. Yu, L. Kuo, and K. Ma (1999), Rapid afterslip following the 1999 Chi-Chi, Taiwan earthquake, *Geophys. Res. Lett.*, *29*(16), 1754, doi:10.1029/2002GL014967.

Jin, D., S.-I. Karato, and M. Obata (1998), Mechanisms of shear localization in the continental lithosphere: Inference from the deformation microstructures from the Ivrea zone, northwest Italy, *J. Struct. Geol.*, *20*, 195–209.

Jónsson, S., P. Segall, R. Pedersen, and G. Björnsson (2003), Post-earthquake ground movements correlated to pore-pressure transients, *Nature*, *424*, 179–183.

Kenner, S. J., and P. Segall (2000), Postseismic deformation following the 1906 San Francisco earthquake, *J. Geophys. Res.*, *105*, 13,195–13,209.

Küster, M., and B. Stöckhert (1999), High differential stress and sublithostatic pore fluid pressure in the ductile regime—Microstructural evidence for short-term post-seismic creep in the Sesia zone, western Alps, *Tectonophysics*, *303*, 263–277.

Langbein, J., and H. Johnson (1997), Correlated errors in geodetic time series: Implications for time-dependent deformation, *J. Geophys. Res.*, *102*, 592–604.

Marone, C. J., C. H. Scholz, and R. Bilham (1991), On the mechanics of earthquake afterslip, *J. Geophys. Res.*, *96*, 8441–8452.

Meade, B. J., B. H. Hager, S. McClusky, R. E. Reilinger, S. Ergintav, O. Lenk, A. Barka, and H. Özener (2002), Estimates of seismic potential in the Marmara sea region from block models of secular deformation constrained by Global Positioning System measurements, *Bull. Seismol. Soc. Am.*, *92*, 208–215.

Melbourne, T. I., F. H. Webb, J. M. Stock, and C. Reigber (2002), Rapid postseismic transients in subduction zones from continuous GPS, *J. Geophys. Res.*, *107*(B10), 2241, doi:10.1029/2001JB000555.

Miyazaki, S., J. J. McGuire, and P. Segall (2003), A transient subduction zone slip episode in southwest Japan observed by the nationwide GPS array, *J. Geophys. Res.*, *108*, 2087, doi:10.1029/2001JB000456.

Montési, L. G. J. (2004), Postseismic deformation and the strength of ductile shear zones, *Earth Planets Space*, in press.

Montési, L. G. J., and G. Hirth (2003), Grain size evolution and the rheology of ductile shear zones: From laboratory experiments to postseismic creep, *Earth Planet. Sci. Lett.*, *211*, 97–110.

Montési, L. G. J., and M. T. Zuber (2002), A unified description of localization for application to large-scale tectonics, *J. Geophys. Res.*, *107*(B3), 2045, doi:10.1029/2001JB000465.

Nishimura, T., et al. (2000), Distribution of seismic coupling on the subducting plate boundary in northeastern Japan inferred from GPS observations, *Tectonophysics*, *323*, 217–238.

Oppenheimer, D. H., W. H. Bakun, and A. G. Lindh (1990), Slip partitioning of the Calaveras fault, California, and prospects for future earthquakes, *J. Geophys. Res.*, *95*, 8483–8498.

Owen, S., G. Anderson, D. Agnew, H. Jonson, K. Hurst, R. Reilinger, Z.-K. Shen, J. Svarc, and R. Baker (2002), Early postseismic deformation from the 16 October 1999 M_w 7.1 Hector Mine, California, earthquake as measured by survey-mode GPS, *Bull. Seismol. Soc. Am.*, *92*, 1423–1432.

Peltzer, G., P. Rosen, F. Rogez, and K. Hudnut (1998), Poroelastic rebound along the 1992 Landers earthquake surface rupture, *J. Geophys. Res.*, *103*, 30,131–30,145.

Poirier, J.-P. (1980), Shear localization and shear instability in materials in the ductile field, *J. Struct. Geol.*, *2*, 135–142.

Pollitz, F. F., R. Bürgmann, and B. A. Romanowicz (1998a), Viscosity of the oceanic asthenosphere inferred from remote triggering of earthquakes, *Science*, *280*, 1245–1249.

Pollitz, F. F., R. Bürgmann, and P. Segall (1998b), Joint estimation of afterslip rate and postseismic relaxation following the 1989 Loma Prieta earthquake, *J. Geophys. Res.*, *103*, 26,975–26,992.

Pollitz, F. F., C. Wicks, and W. Thatcher (2001), Mantle flow beneath a continental strike-slip fault: Postseismic deformation after the 1999 Hector Mine earthquake, *Science*, *293*, 1814–1818.

Press, W. H., S. A. Teukolsky, W. T. Vetterling, and B. P. Flannery (1992), *Numerical Recipes in FORTRAN 77, The Art of Scientific Computing*, 2nd ed., Cambridge Univ. Press, New York.

Ramsay, J. G. (1980), Shear zone geometry, a review, *J. Struct. Geol.*, *2*, 83–99.

Regenauer-Lieb, K., and D. A. Yuen (2003), Modeling shear zones in geological and planetary sciences: Solid- and fluid-thermal-mechanical approaches, *Earth Sci. Rev.*, *63*, 295–349.

Reilinger, R. E., et al. (2000), Coseismic and postseismic fault slip for the 17 August 1999, M = 7.5, İzmit, Turkey earthquake, *Science*, *289*, 1519–1524.

Rice, J. R., and A. L. Ruina (1983), Stability of steady frictional slipping, *J. Appl. Phys.*, *50*, 343–349.

Ruina, A. L. (1983), Slip instability and state-variable friction laws, *J. Geophys. Res.*, *88*, 10,359–10,370.

Savage, J. C., and J. L. Svarc (1997), Postseismic deformation associated with the 1992 M_w = 7.3 Landers earthquake, southern California, *J. Geophys. Res.*, *102*, 7565–7577.

Savage, J. C., M. Lisowski, and J. L. Svarc (1994), Postseismic deformation following the 1989 (M = 7.1) Loma Prieta earthquake, *J. Geophys. Res.*, *99*, 13,757–13,765.

Scholz, C. H. (2002), *The Mechanics of Earthquakes and Faulting*, 2nd ed., Cambridge Univ. Press, New York.

Segall, P., R. Bürgmann, and M. Matthews (2000), Time-dependent triggered afterslip following the 1989 Loma prieta earthquake, *J. Geophys. Res.*, *105*, 5615–5634.

Shen, Z.-K., D. D. Jackson, Y. Feng, M. Cline, M. Kim, P. Fang, and Y. Bock (1994), Postseismic deformation following the Landers earthquake, California, 28 June 1992, *Bull. Seismol. Soc. Am.*, *84*, 780–791.

Sibson, R. H. (1980), Transient discontinuities in ductile shear zones, *J. Struct. Geol.*, *2*, 165–171.

Sibson, R. H. (1986), Earthquakes and rock deformation in crustal shear zones, *Annu. Rev. Earth Planet. Sci.*, *14*, 149–175.

Smith, R. B. (1977), Formation of folds, boudinage, and mullions in non-Newtonian materials, *Geol. Soc. Am. Bull.*, *88*, 312–320.

Stein, R. S. (1999), The role of stress transfer in earthquake occurrence, *Nature*, *402*, 605–609.

Stesky, R. M., W. F. Brace, D. K. Riley, and P.-Y. F. Robin (1974), Friction in faulted rock at high temperature and pressure, *Tectonophysics*, *23*, 177–203.

Trepmann, C., and B. Stöckhert (2003), Quartz microstructures developed during non-steady state plastic flow at rapidly decaying stress and strain rate, *J. Struct. Geol.*, *25*, 2035–2051.

Tse, S. T., and J. R. Rice (1986), Crustal earthquake instability in relation to the depth variation of frictional slip properties, *J. Geophys. Res.*, *91*, 9452–9472.

Uchida, N., T. Matsuzawa, A. Hasegawa, and T. Igarashi (2003), Interplate quasi-static slip off Sanriku, NE Japan, estimated from repeating earthquakes, *Geophys. Res. Lett.*, *30*(15), 1801, doi:10.1029/2003GL017452.

Vauchez, A., and A. Tommasi (2003), Wrench faults down to the asthenosphere: Geological and geophysical evidence and thermo-mechanical effects, in *Intraplate Strike-Slip Deformation Belts*, edited by F. Storti, R. E. Holdsworth, and F. Salvini, *Geol. Soc. Spec. Publ.*, *210*, 15–34.

White, S. H., and R. J. Knipe (1978), Transformation and reaction-enhanced ductility in rocks, *J. Geol. Soc. London*, *165*, 513–516.

Yagi, Y., M. Kikuchi, and T. Sagiya (2001), Co-seismic slip, post-seismic slip, and aftershocks associated with two large earthquakes in 1996 in Hyuga-nada, Japan, *Earth Planets Space*, *53*, 793–803.

Yu, S., Y. Hsu, L. Kuo, H. Chen, and C. Liu (2003), GPS measurement of postseismic deformation following the 1999 Chi-Chi, Taiwan, earthquake, *J. Geophys. Res.*, *108*(B11), 2520, doi:10.1029/2003JB002396.

Zweck, C., J. T. Freymueller, and S. C. Cohen (2002), The 1964 Alaska earthquake: Present day and cumulative postseismic deformation in the western Kenai peninsula, *Phys. Earth Planet. Inter.*, *132*, 5–20.

L. G. J. Montési, Department of Geology and Geophysics, Woods Hole Oceanographic Institution, MS 24, Woods Hole, MA 02543-1542, USA. (montesi@whoi.edu)